Helsinki University of Technology
Department of Engineering Physics and Mathematics
Materials Physics Laboratory

Master's Thesis

Momentum Transfer between Quantum Gases

Juha Vartiainen

Supervisor: prof. Martti M. Salomaa
Instructor: prof. Martti M. Salomaa

Espoo
24th January 2002

HELSINKI UNIVERSITY OF TECHNOLOGY
DEPARTMENT OF ENGINEERING PHYSICS AND MATHEMATICS

ABSTRACT OF MASTER'S THESIS

Author:	Juha Vartiainen
Department:	Department of Engineering Physics and Mathematics
Major subject:	Materials Physics
Minor subject:	Information Technology
Title:	Momentum Transfer between Quantum Gases
Title in Finnish:	Liikemäärän vaihto kvanttikaasujen välillä
Chair:	Tfy-44 Materials Physics
Supervisor:	Prof. Martti M. Salomaa
Instructor:	Prof. Martti M. Salomaa

Abstract:

In this Master's Thesis, we consider the properties of interpenetrating atomic gases at low temperatures, apply the linear response theory to calculate the momentum transfer between them, and review recent experimental result. This work is motivated by the rapid development in experimental research, which has been awarded with Nobel Prizes in 1997 and 2001.

The laser cooled and magneto-optically trapped atomic gases are dilute. At low-temperatures, the shape and the optical properties of the trapped gas reflect the effects of quantum mechanical many-body phenomena. The gases are controlled with high precision using both the electromagnetic and gravitational fields. The experiments have yielded information on the properties of degenerate gases and Bose-Einstein condensate. In the future, one possible goal is the observation of the predicted BCS transition in Fermi gases. Based on the experience with atomic gases, many experiments and applications of matter-wave optics are currently proposed and also pursued *e.g.*, Bragg diffraction and an atom laser.

Theoretical work on atomic gases is relatively straightforward due to the diluteness and the weakness of the interactions. We derive the dynamic structure factor for an impurity particle, and for classical and quantum ideal gases using linear response theory. The mobility of an impurity particle and the momentum transfer between the gases is expressed using the dynamic structure factor. The temperature dependence of these quantities is considered. In the low-temperature limit, the differences arising from quantum statistics are established.

The methods used and the result obtained in this work may be applied to fundamental research of physics. Detailed knowledge on impurity motion and the momentum transfer between the gases is essential in cooling and manipulating samples of degenerate atomic gases.

Number of pages: 55 Keywords: quantum gas, mobility, momentum transfer

Department fills

Approved: Library code:

TEKNILLINEN KORKEAKOULU
TEKNILLISEN FYSIIKAN JA MATEMATIIKAN OSASTO

DIPLOMITYÖN TIIVISTELMÄ

Tekijä:	Juha Vartiainen
Osasto:	Teknillisen fysiikan ja matematiikan osasto
Pääaine:	Materiaalifysiikka
Sivuaine:	Informaatiotekniikka
Työn nimi:	Liikemäärän vaihto kvanttikaasujen välillä
Title in English:	Momentum Transfer between Quantum Gases
Professuurin koodi ja nimi:	Tfy-44 Materiaalifysiikka
Työn valvoja:	Prof. Martti M. Salomaa
Työn ohjaaja:	Prof. Martti M. Salomaa

Tiivistelmä:

Tässä diplomityössä käsitellään atomikaasujen ominaisuuksia matalissa lämpötiloissa, sovelletaan lineaarista vasteteoriaa niiden laskemiseksi sekä esitellään viimeaikaisia koetuloksia. Työn motivaationa on viime vuosien huikea edistys alan kokeellisessa tutkimuksessa, josta on myönnetty fysiikan Nobelin palkinto vuosina 1997 ja 2001.

Laser-jäähdytetyt ja magneto-optisesti vangitut atomikaasut ovat hyvin harvoja. Matalissa lämpötiloissa nähdään vangittujen kaasujen ulkomuodossa ja optisissa ominaisuuksisa piirteitä, jotka voidaan selittää kvanttimekaanisilla monihiukkasilmiöillä. Kaasujen tilaa voidaan kontrolloida hyvin tarkasti sähkömagneettisen- ja painovoimakentän yhteisvaikutuksella. Tähänastiset kokeet ovat keskittyneet degeneroituneiden kaasujen ominaisuuksien ja Bose-Einsteinin kondensaatin tutkimukseen. Tulevien kokeiden yksi mahdollinen päämäärä on BCS-transition havaitseminen Fermi-kaasuissa. Atomikaasuista saatujen kokemusten perusteella on ehdotettu ja toteutettu useita aineaalto-optisia kokeita ja sovelluksia, kuten Braggin sironta ja atomilaser.

Atomikaasujen harvuudesta ja atomien välisten vuorovaikutusten heikkoudesta johtuen niiden teoreettinen käsittely on verrattaen suoraviivaista. Työssä johdetaan dynaaminen rakennetekijä epäpuhtaushiukkaselle sekä klassiselle ja kvanttikaasulle käyttäen lineaarisen vasteen teoriaa. Epäpuhtaushiukkasen liikkuvuus ja kaasujen välinen liikemäärän siirto lausutaan dynaamisen rakennetekijän avulla. Edellä mainittujen suureiden lämpötilariippuvuutta tarkastellaan, ja havaitaan kvanttistatistiikasta johtuva ero matalan lämpötilan rajalla.

Työssä sovellettuja menetelmiä ja saatuja tuloksia voidaan käyttää fysiikan perustutkimukseen. Tiedot epäpuhtauksien liikkuvuudesta ja kaasujen keskinäinen liikemäärän siirtonopeudesta ovat olennaisia degeneroituneiden atomikaasujen jäähdyttämisessä ja käsittelyssä.

Sivumäärä: 55 Avainsanat: kvanttikaasu, liikkuvuus, liikemäärän vaihto

Täytetään osastolla

Hyväksytty: Kirjasto:

Acknowledgements

This Master's Thesis research was carried out in the Materials Physics Laboratory at Helsinki University of Technology. I would like to thank professor Martti M. Salomaa for providing me the opportunity to perform this work, for suggesting the topic, for experienced advice, and for his fruitful suggestions for improvements to the manuscript. In the Materials Physics Laboratory, I have been given excellent working conditions and an inspiring atmosphere; for these I want to thank all the laboratory personnel. Finally, I want to thank my parents for encouraging me to pursue these studies.

Espoo, 24th January 2002

Juha Vartiainen

Contents

1 Introduction

This Master's Thesis is motivated by the recent breakthroughs in the study of laser cooling [1, 2, 3] and its application to the production and study [4] of Bose-Einstein condensation (BEC) in dilute atomic gases [5]. Despite the Nobel Prices awarded (Steven Chu, Claude Cohen-Tannoudji and William D. Phillips in 1997, and Eric A. Cornell, Wolfgang Ketterle, and Carl E. Wieman in 2001), much research remains ahead. One can name at least one well-formulated goal not reached yet, the Fermi condensate, which would be a degenerate Fermi gas in a pair-correlated BCS-like state. Here, using linear response theory [6], we consider the temperature dependence of the rate of momentum transfer between two atomic gases and the motion of an impurity immersed to a quantum gas. In the low-temperature limit, we obtain power-law behaviours which reflect the effects of fundamental quantum physics: bosonic stimulation and Pauli blocking.

Since 1911 — the times of Kamerlingh Onnes — low-temperature phenomena have intrigued physicists. The collective behavior of ensembles of atoms, arising from fundamental quantum-mechanical effects, becomes dominant when thermal motion is suppressed. The early developments of low-temperature physics were largely based on the properties of liquid helium. A first signal of Bose-Einstein condensation (BEC) was encountered in the λ-transition of liquid ^{4}He. However, helium is a liquid at low temperatures over most of the phase diagram. Consequently, no microscopic theory exists for superfluid ^{4}He due to the presence of the strong interparticle interactions.

In recent years, rapid progress in novel experimental techniques to cool and to manipulate a dilute gas of atoms has generated a whole new branch of fundamental research. With the help of laser cooling, one may slow down atoms and trap them into a magneto-optical trap (MOT). By further evaporative cooling, one reaches temperatures well below 1 μK. In degenerate dilute atomic gases, the interparticle interactions are weak. Therefore, the dilute gases are amenable to theoretical treatment and they allow for quantitative tests of microscopic theo-

ries using the tools and precision of atomic-physics experiments [7, 8]. Research on the atomic gases was highlighted by the observation of Bose-Einstein condensation in the dilute cloud of Rubidium-87 atoms in 1995.

Short-term applications of the results of this research are purely scientific. Theories of many-body quantum physics may be tested to an unprecedented accuracy. Medium-term applications may consist of precision measurements and novel tools for nanotechnology [9]. The Fermi s-wave suppression is proposed as a natural way to avoid collisional frequency shifts in atomic clocks. Interferometrical measurements with matter waves may become possible. In the long run, the applications are unknown, just as they were for the laser in 1960. The atom laser, a coherent beam of matter waves, is one novel device based on the extraordinary properties of ultracold atom gases [10, 11, 12]. The atom laser and other atom-optical instruments may have far-reaching applications.

This Master's Thesis is organized as follows. In Sec. 2, we review the properties of dilute atomic gases at low temperatures and discuss spectral measurements. Section 3 extends the above discussion to linear response theory. The connections between various linear-response functions are reviewed. One of these functions, the dynamic structure factor $S(\mathbf{k}, \omega)$ is studied at greater detail. An analytic expression for $S(\mathbf{k}, \omega)$ is derived for classical and quantum gases. In Sec. 4, the momentum transfer between interpenetrating quantum systems is calculated using methods developed in the earlier Chapters. The quantum system may be an impurity, an ideal gas governed by the classical Maxwell-Boltzmann, or the quantal Bose-Einstein or Fermi-Dirac statistics. Our formulation of the expression for the momentum transfer is quite general. The formalism may as well be applied to systems quite different from atomic gases: for example one finds the Coulombic drag between two nearby electron gases calculated using the same ideas [13]. Finally, a summary and conclusions are presented in Sec. 5.

2 Experiments on atomic gases

2.1 Atomic gases

Let us consider a gas of neutral atoms interacting via a binary short-range potential $V(\boldsymbol{r})$. At high enough temperatures and low enough pressures, the gas is dilute. Each atom moves as if it were essentially free, apart from infrequent collisions with the other atoms or with the container walls. The system is well described by the kinetic theory of gases [14]. As pressure is increased and temperature is lowered, the above picture tends to break down. Because of the increase in density, the interactions between the particles become more intensive. At some stage, the gas undergoes a phase transition into the liquid state. In this work, we discuss experiments in which, using sophisticated methods, one does not allow the phase transition to begin. Thus the system may be cooled in the metastable gaseous state dowb to temperatures where macroscopic quantum effects become manifest.

The quantum effects arise from the symmetry properties of the many-body wave functions, and are essentially statistical in their nature. We are thus led to consider the quantum mechanics in atomic gases. Usually one does not have to take the quantum effects into account at room temperature. They only become important when the thermal de Broglie wavelength

$$\lambda_{\mathrm{dB}} = \frac{\hbar}{\sqrt{2mk_{\mathrm{B}}T}} \tag{2.1}$$

becomes comparable to the average spacing between the particles. For the alkali-metal atoms, the relevant temperature region is below 1 μK.

An atom consists of electrons, protons, and neutrons. Furthermore, the protons and neutrons consist of more elementary particles, quarks. However, when an atom exchanges energy whose characteristic wavelength is longer than the radius of the atom, it behaves as a single particle. The atom has a quantized

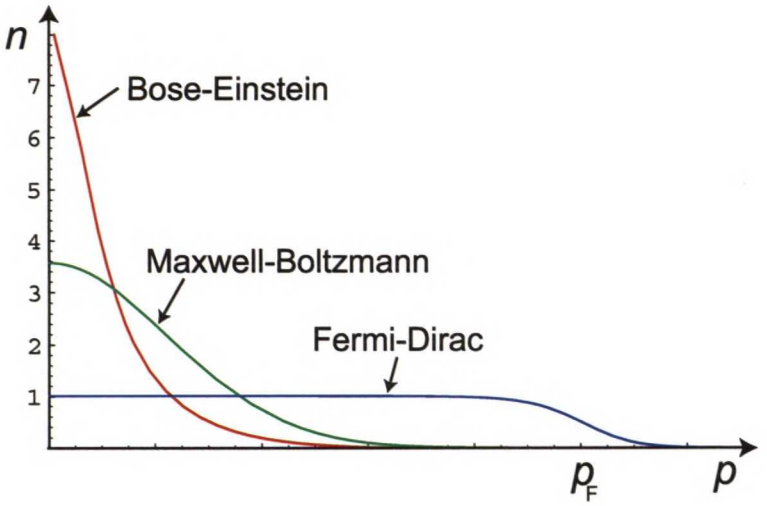

Figure 2.1: Differences between classical and quantal distribution functions at low temperatures.

total spin, which may be an integer or a half-integer, depending on the number of the half-integer-spin constituents. The particles with integer spin are called bosons and particles with half-integer spin are called fermions.

Bosons and fermions display quite different properties at low temperatures. Using the methods of statistical physics [14], one obtains the distribution function

$$n_{\boldsymbol{p}} = \frac{1}{e^{\beta(\epsilon-\mu)} \pm 1}, \tag{2.2}$$

which describes the probability that a single particle in thermal equilibrium has the energy ϵ. In Eq. (2.4), the $\pm$ sign stands for fermions (bosons), $\epsilon = \epsilon(\boldsymbol{p})$, $\beta = k_{\mathrm{B}}T$ and k_{B} is Boltzmann's constant. The chemical potential $\mu = \mu(T)$ is adjusted to yield the correct total number of particles in the system

$$N = \int d\boldsymbol{p}\, n_{\boldsymbol{p}}. \tag{2.3}$$

In the low-temperature limit, μ vanishes for bosons, and it approaches a constant value ϵ_{F}, called the Fermi energy, for fermions. In the high-temperature limit, μ is highly negative and $n_{\boldsymbol{p}}$ reduces to the Maxwell-Boltzmann distribution for a classical gas

$$n_{\boldsymbol{p}} = e^{-\beta(\epsilon-\mu)}. \tag{2.4}$$

Differences between the distribution functions of ideal degenerate Fermi-Dirac, Bose-Einstein, and Maxwell-Boltzmann gases are illustrated in Fig. 2.1.

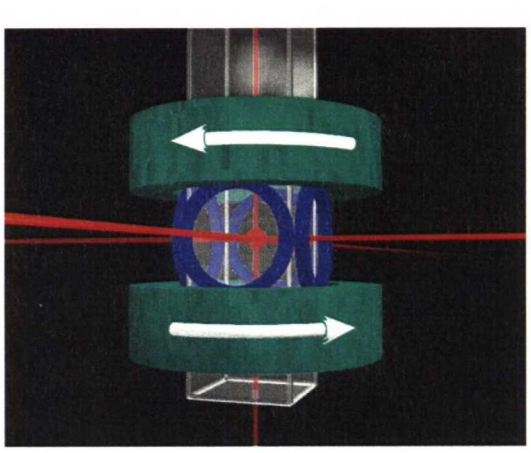

(a) Schematic of a magneto-optic trap. The green magnets create a bowl potential and the six-directional laser beams are used to slow down the atoms, which are in the vacuum chamber (glass box in the center of the trap). The almost transparent atomic gas does not warm due to radiation unless the setup is at room temperature. The image is from Ref. [68].

(b) Principle of evaporative cooling. The hottest atoms have enough energy to escape the trap. This leads to the cooling of the sample. After the gas is rethermalized, the trapping potential is lowered and the process repeats itself. Eventually, only a fraction of the atoms is lost, but the temperature is lowered through several orders of magnitude.

Figure 2.2: Trapping and cooling of atomic gases.

Using the recently established procedures, an atomic gas may be cooled to temperatures near the degeneracy regime. In a typical experiment, the atomic sample is first precooled optically and then loaded into a magneto-optic trap, see Fig. 2.2(a). The cooling then proceeds by evaporation, *i.e.*, the removal of the most energetic atoms and subsequent rethermalization of the gas via elastic collisions, see Fig. 2.2(b). To achieve yet lower temperatures, many sophisticated variants of the methods have been developed, but we do not concentrate on the experimental techniques here. A detailed discussion is given in Refs. [1, 2, 3]. In the part of the phase diagram corresponding to the conditions of MOT, the ground state of the atomic sample is liquid or solid. The technique to prevent the phase transition into the liquid or solid state is to keep the gas so dilute that collisions are predominantly binary. In binary collisions, no molecules are formed due the momentum conservation. However, the state is unstable and the sample prepared is lost in a few seconds.

The ultracold atomic gas in a magneto-optic trap constitutes a dilute system

in which the interparticle interactions are weak and readily treated theoretically. Experiments indicate that the properties of atomic gases are very nearly those of an ideal gas [15]. Furthermore, detailed tuning of the sign and strength of the interactions is possible, for example, through the Feshbach resonances in a magnetic field [16].

The interactions between the atoms in the dilute gases are either s-wave or p-wave in nature. These waves are the first two terms in the series of spherical harmonics, and there may be also contributions from the d-, f- and higher-order waves. If the interactions are weak, the s-wave contribution is usually dominant. However, when the s-wave contribution is suppressed, one must take the p-wave contribution into account.

2.1.1 Degenerate Bose gases

Some of the elementary particles, such as gluons and mesons, are bosons. Here we discuss an alkali metal (^{87}Rb, ^{23}Na, and ^{7}Li) vapor of atoms that has bosonic features and is suitable for the dilute-gas cooling experiments [5, 17].

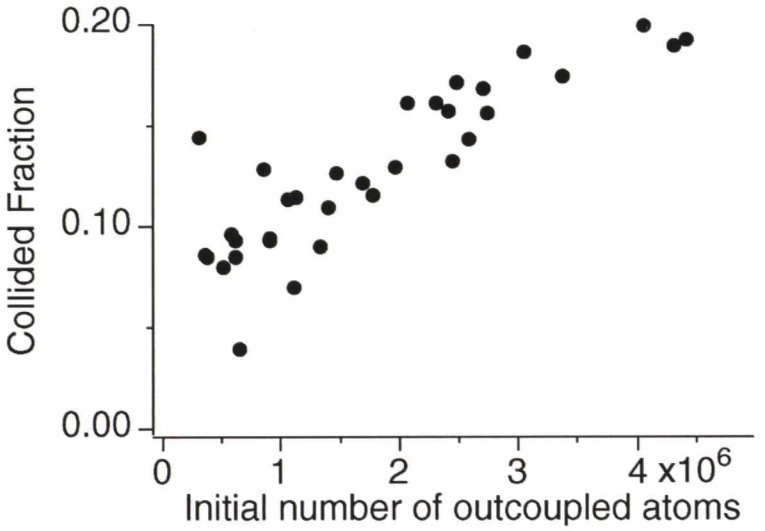

Figure 2.3: Enhancement of scattering out of BEC due to the occupation of the final state. The graph is from Ref. [19].

The trapping and cooling of bosonic atoms into the degeneracy regime is relatively easy using the magneto-optic trapping and evaporative cooling. At low temperatures, the elastic collisions between the atoms are predominantly s-wave-like in character [18]. The scattering is isotropic. Thus the rethermalization of

the sample of Bose gas is relatively fast. To avoid losses due to spin-exchange collisions, typically only atoms in a single spin state are loaded into the trap.

A characteristic feature for the degenerate Bose system is bosonic stimulation. It enhances the scattering into already occupied states, like in la laser, see Fig. 2.3. At low temperatures, this tendency leads to most interesting phenomena in a degenerate Bose gas: the Bose-Einstein phase transition in which a macroscopic number of atoms occupy the ground state.

2.1.2 Bose-Einstein condensate

When a gas of bosonic atoms is cooled below its BEC transition temperature, it profoundly changes its properties. The appearance of a macroscopically occupied ground state leads to a variety of new phenomena, which set Bose-Einstein condensates apart from all other substances. Recent experiments include, for example, the enhancement and suppression of elastic collisions of impurity atoms [19], the suppression of dissipation due to superfluidity [20], and the enhancement and suppression of the scattering of light [21]. In addition, the BEC features many other peculiar properties that shall not be discussed here due to lack of space, see Fig. 2.4(b).

A Bose-Einstein condensate displays special ordering. Thus it has in principle a peak spectrum in scattering experiments. However, a BEC has density fluctuations similar to a classical ideal gas [22]. For electromagnetic waves, these density fluctuations cause Rayleigh scattering. In close analogy, if a matter wave propagates through a condensate, there will occur elastic scattering. This leads to broadening of the spectral lines.

For the long-wavelength perturbations, there is a new effect compared to classical systems, namely superfluidity. Superfluidity arises from the phonon-like energy-momentum dispersion relation of the BEC. It does not allow for the generation of elementary excitations below the Landau critical velocity v_C thus implying dissipationless flow. One may interpret this suppression of scattering as the "reluctance" of a condensate against long-wavelength modulations.

2.1.3 Degenerate Fermi gases

Fermions, such as electrons, protons, and neutrons, compose all of the matter around us, and phenomena derived from the quantum degeneracy of fermions are omnipresent in Nature. The behavior of a degenerate Fermi gas is remarkably different from that of a degenerate Bose gas. The structure and behavior of

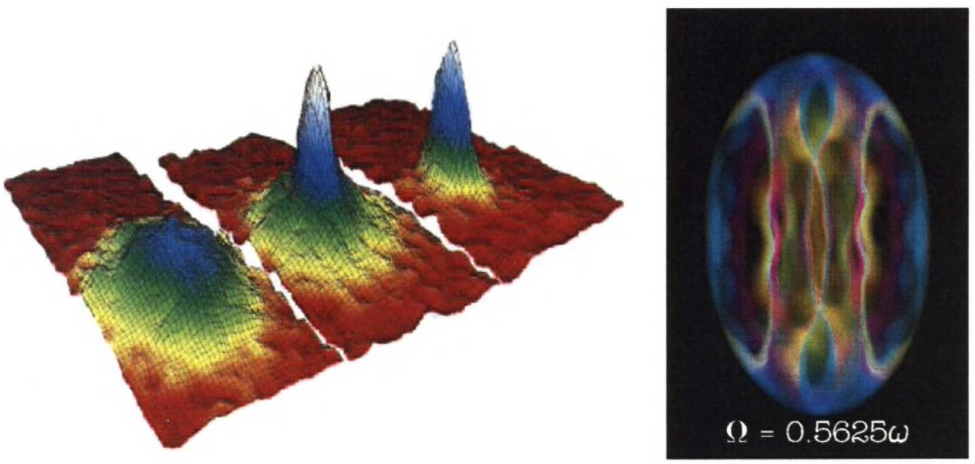

(a) First realization of BEC in the MOT. Temperature decreases in the images from the left to the right. The condensation is manifested as the sharp peak in the spatial and momentum distribution of the atoms. The image is from Ref. [69].

(b) Computed false-color image of a vortex in a BEC. The image is from Ref. [70].

Figure 2.4: Two characteristic properties of Bose-Einstein condensates.

such diverse systems as atoms, nuclei, electrons in metals, white dwarfs, and neutron stars is governed by Fermi-Dirac statistics. All the multitude of different properties of these systems reflect the Pauli exclusion principle, which prevents two fermions from sharing the same quantum state.

Fermi systems are in general dense and strongly interacting. Until recently, there were only few low-density Fermi systems, *e.g.*, a dilute solution of liquid ^{3}He dissolved in superfluid ^{4}He and the Wigner crystal of electrons on the surface of liquid helium (2D system). Reaching temperatures below the Fermi temperature T_F in atomic fermion gases is experimentally difficult. Indeed, no s-wave scattering is allowed for identical fermions, and due to the centrifugal barrier [23] the p-wave cross section vanishes as T^2 for decreasing temperature T. Relying on elastic collisions, evaporative cooling fails for fermions [24].

Only a few experiments on the cooling and trapping of fermionic atoms have been reported. However, they have enabled new opportunities for studying fundamental quantum-statistical and many-body physics. In Ref. [27], trapped ^{40}K atoms were cooled down to temperatures below $0.5\,T_\mathrm{F}$ at which the Fermi degeneracy sets in, see Fig. 2.5. Two lithium isotopes were trapped simultaneously in a magneto-optical trap in Ref. [11] and cooled down to $0.25\,T_\mathrm{F}$ [28]. More recently,

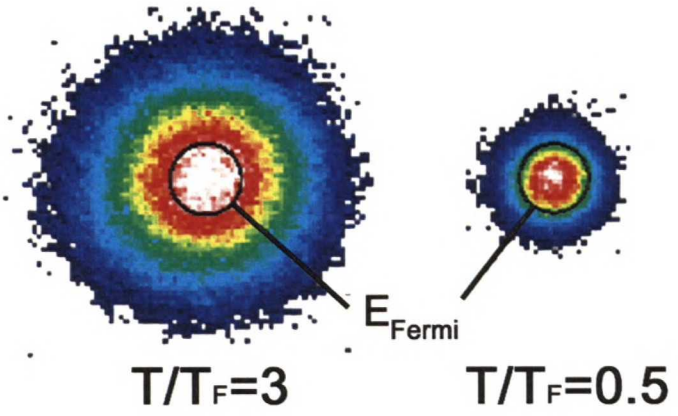

Figure 2.5: Images of an ultracold gas of ^{40}K atoms in a magnetic trap. The Pauli exclusion principle prevents an arbitrarily high atomic density at the center of the trap. The image is from Ref. [67].

the same temperature was obtained using ^{6}Li in a bosonic ^{23}Na bath [29]. The purely optical trapping of fermionic lithium has been achieved as well [30].

The experimentally observed [15] quantum-statistical suppression of s-wave interactions between identical fermions renders the cooling of a fermionic sample difficult. It also serves to make an ultracold trapped Fermi gas an excellent realization for an ideal gas. In Ref. [31], the collisional Pauli blocking is observed through a measurement of the thermal relaxation rate in ^{40}K, see Fig. 2.6.

The most promising cooling technique for fermions seems to be sympathetic cooling, which is based on Bose-Fermi mixtures. The sympathetic cooling allows one to overcome the limitations in the cooling of a Fermi gas. It employs a buffer gas to cool another species via collisions. If bosonic atoms as well as fermionic atoms are loaded into a magnetic trap, the bosons can be cooled evaporatively while the fermions will be cooled sympathetically via elastic s-wave collisions with the bosons. A second alternative is to load two species of fermionic atoms into the trap, allowing elastic s-wave collisions between the different fermions to rethermalize the gas during evaporative cooling. The same cooling strategy also work for two spin states of the same Fermi gas. An analysis of resonant absorption images, similar to that used to investigate Bose-Einstein condensates, may be used after the evaporation.

To broaden the discussion of the fermion cooling, one may note that many other cooling methods have also been proposed, but experimental results on these have not been reported yet. For example, a promising candidate for a cooling method called Raman cooling [32] utilizes adjusted spontaneous Raman-emission

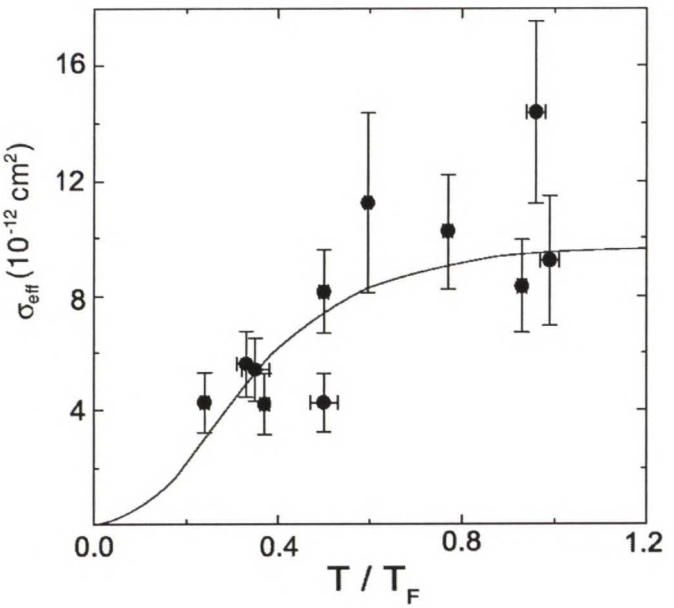

Figure 2.6: Experimental evidence of collisional Pauli blocking in ^{40}K. At $0.4\,T_F$, the effective elastic cross section is observed to be roughly a factor of two smaller than that above the Fermi temperature, T_F. The solid curve shows the result of a quantum-kinetic calculation of the collision rate. Graph from Ref. [31].

rates and an appropriately designed anharmonic trap.

A degenerate Fermi gas is expected to feature many interesting phenomena in its thermodynamics, excitation spectrum, collisional dynamics, and the scattering of light [33]. Several authors focus on the interaction of the atomic cloud with light: modifications of the refractive index or the absorption coefficient of the gas [34, 35], reduction of the spontaneous-emission rate of the excited atoms in the atomic cloud, and the angular dependence of the radiation pattern [36].

Due to the Pauli principle, the distribution function of the degenerate Fermi gas does not vary appreciably when temperature is varied. Thus, the determining of the temperature of a fermionic sample is difficult. Diagnostics of Fermi degeneracy of a trapped gas involve the study of its spatial distribution, either for a pure fermionic sample, or with the presence of a Bose-Einstein condensate [28]. These methods are useful in the temperature regime $T \gtrsim T_F$, but become less sensitive in the strongly degenerate regime where $T \ll T_F$ [37]. To gain information on the degeneracy of Fermi gas at $T \ll T_F$, one can make use of of inelastic processes as pointed out in [36].

Although the lack of interparticle interactions makes the theoretical interpre-

tation straightforward and may facilitate precision measurements, a richer set of phenomena can emerge in a dilute interacting system. The predicted phenomena for an interacting atomic Fermi gas include zero sound [38], suppression of elastic collisions [36], and component separation [40]. A major goal is to observe the predicted [41] BCS transition for fermionic atoms. As a scientific achievement, this would compare with the experimental realization of atomic Bose-Einstein condensates.

2.1.4 Fermi condensate

There exists no such condensate of fermions as there is for bosons. However, an especially fascinating property of Fermi gases is that with an effectively attractive interaction between the particles, the ground state of the system may become unstable with respect to the formation of bound pairs of quasiparticles. The pairs, analogous to the Cooper pairs of electrons in a superconductor, acquire bosonic character and form a condensate [27] through the Bardeen-Cooper-Schrieffer (BCS) phase transition. Theoretical studies have suggested that this fermionic condensate will only occur at very low temperatures [40].

Studies of degenerate Fermi gases [28, 30, 31, 32] presently face bottlenecks for reaching temperatures low enough to form Cooper pairs. Below the Fermi temperature, evaporative cooling of a dual Fermi gas begins to stall as the nearly fully occupied low-energy states exhibit Pauli blocking [39]. In a mixture of Fermi and Bose gases, the sympathetic cooling provided by ultracold bosons loses efficiency when the bosonic heat capacity falls below its fermionic counterpart [28]. The lowest temperatures achieved are thus about a fourth of the Fermi temperature, whereas Cooper-pair formation requires a temperature of at least an order of magnitude lower [40, 41]. However, by adjusting the interatomic interactions using Feshbach resonances, rf microwave fields, dc electric fields, or photoassociation, it may become feasible to raise the BCS transition temperature to an experimentally accessible regime [42].

The BCS phase transition arises from the pairing of electrons on the Fermi surface, which creates a gap in the energy spectrum. To make such pairing to work, an effective attraction between the atoms is required. For bosons, an attractive interaction corresponds to a negative s-wave scattering length. As mentioned above, the Pauli exclusion principle prohibits s-wave scattering of fermionic atoms into identical quantum states. This leaves only p-wave collisions as a pairing mechanism, but the resulting interactions are energetically suppressed and are generally considered to yield experimentally unattainable pairing transition temperatures [16].

The recent proposals [40] suggest that the p-wave interactions may be enhanced by the application of very large dc electric fields, which can be generated with powerful CO_2 lasers. A second possibility is to use two different spin states of a fermionic atom, thus restoring s-wave collisions as a pairing mechanism. In this context, ^{6}Li appears to be a promising candidate, since it has a large negative s-wave scattering length $a = -2160\, a_0$, in units of the Bohr radius a_0. The critical temperature for Cooper pairing through s-wave scattering is approximately [40]

$$T_c \sim \frac{E_F}{k_B} \exp\left(-\frac{\pi}{2k_F|a|}\right), \tag{2.5}$$

where E_F and k_F are the Fermi energy and momentum, respectively. As pointed out in Ref. [40], for experimentally realizable Fermi energies $E_F/k_B \sim 600$ nK, the critical temperature would be $T_c \sim 15$ nK for ^{6}Li. Thus any alkali metal gas with an equally large, negative scattering length should be a viable candidate for Cooper pairing.

It still is an open question how to observe the predicted BCS transition. The observation poses a double challenge [48]. The energy gap is expected to be small, thus a sensitive probe has to be found. Furthermore, the trapping potential leads to the appearance of low-energy subgap excitations, which may complicate resolving the gap energy.

The effects of Cooper pairing may be understood in terms of enhanced incoherent scattering processes, resulting in an increased optical linewidth, a line shift, and an increase in the static structure factor. This is because due the BCS pairing, atoms and holes near the Fermi surface are mixed; for a given recoil momentum there exist more unoccupied states into which the atoms can scatter. These optical processes could possibly signal the presence of a pair-correlated state and determine the value of the BCS order parameter in a dilute Fermi gas.

There are several proposals for measuring the superconducting order parameter. The optical response of a superfluid state in a zero-temperature Fermi gas is studied in Ref. [46], and as a result a strong dependence of the Bragg diffraction rate on the BCS order parameter is suggested. Off-resonant light scattering and Fourier-imaging techniques are proposed in Ref. [45]. Superfluidity is predicted to broaden the spectral lines of the scattered light [33, 47]. Laser probing of the Cooper-paired trapped atoms is discussed in Ref. [48].

2.2 Bragg spectroscopy

In this Section we consider the diffraction of atoms by means of light-stimulated transitions of photons between two non-parallel laser beams, see Fig. 2.7(a). When a coherent atomic beam interacts with a periodic potential formed by a standing light wave it Bragg diffracts, analogous to the Bragg diffraction of X-rays from a crystal.

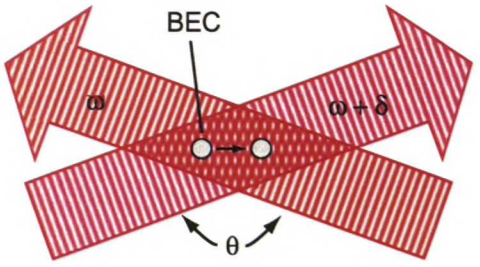

(a) Schematic of the Bragg-diffraction experiment setup. Two detuned, nearly counterpropagating laser beams are applied to the BEC.

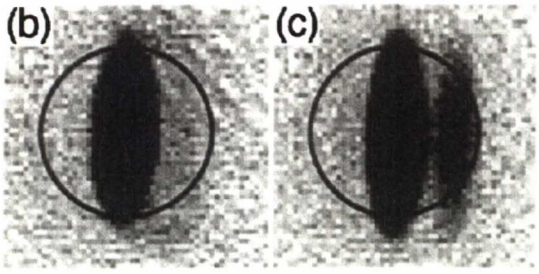

(b) In the first image, a BEC in a magneto-optical trap. In the second image, a splitted BEC obtained as the result of the experiment in Fig. 2.7(a). The image is from Ref. [21].

Figure 2.7: Bragg-diffraction experiments on Bose-Einstein condensates.

The Bragg scattering of X-rays from crystal planes was demonstrated by W. H. Bragg and his son W. L. Bragg in 1912, in a series of pioneering experiments which won them the Nobel Prize in 1915. The experiments [50] on cold atoms present the experimental observation of Bragg scattering of matter waves from a standing-wave crystal of light. This observation provides a beautiful example of the complementarity of particles and waves: the atomic cloud is treated as a wave and the spatially varying laser field as forming the crystal planes, see Fig. 2.8.

The Bragg scattering of atoms from a light grating was first demonstrated in 1988 [50]. Shortly thereafter, it was found to be a breakthrough in the coherent manipulation of atoms. It has been used to manipulate atomic samples in an atom interferometer [25], to split a BEC in Ref. [51], see Fig. 2.7(b), and to perform spectroscopic measurements on a BEC [49, 21]. Small-angle Bragg scatterings, called recoil-induced resonances, have been used for thermometry of laser-cooled atoms [26].

Bragg spectroscopy is an important experimental method since it yields,

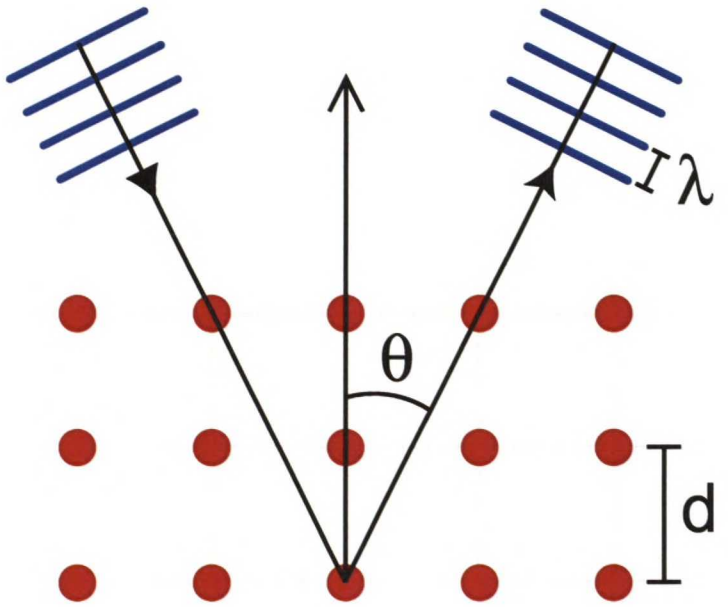

Figure 2.8: Bragg diffraction from a periodic lattice.

among other things, a direct observation of atomic motion within a quantum degenerate gas and provides a quantitative measure of long-range quantum coherence. An analogue of the Bragg scattering of atomic gases is the neutron scattering on the helium liquids at low temperatures [52]. Neutron scattering has provided much important information on the role of collective excitations, the way in which single-particle properties are affected by correlations, and the nature of quantum effects in general.

In the Bragg-diffraction experiment, the two intersecting laser beams create a moving standing wave with a periodic intensity modulation $I(\boldsymbol{r}, t) = I_0 \cos(\Delta\boldsymbol{k} \cdot \boldsymbol{r} - \omega t)$. The intensity modulation creates an optical potential that couples to the local number density of the ground-state atoms [46]. It is assumed that the internal sublevel of the ground-state atom does not change in the scattering process. In a system without fluctuations ($\delta\rho(\boldsymbol{q}) = 0$, where $\rho(\boldsymbol{q})$ is the Fourier transform of the particle density), there is only scattering when the stationary density modulation allows for a momentum transfer at the wavevector $\boldsymbol{q}$ and the incident particles fulfill the Bragg condition

$$N\lambda = 2d\sin(\theta), \tag{2.6}$$

where λ is the wavelength, d is the periodicity of the lattice, θ is the scattering angle, and $N \in \mathbb{N}$ is the order of the Bragg scattering as illustrated in Fig. 2.8.

Another view of the same process is to consider it as a stimulated two-photon exchange that connects two momentum states of the same ground state of the atoms. The absorption of N photons from one laser beam and the stimulated emission into a second beam constitutes a Bragg-scattering process of the Nth order. The process leads to a momentum transfer $\boldsymbol{q}$ and an energy transfer $\hbar\omega$ given by

$$|\boldsymbol{q}| = 2N\hbar|\boldsymbol{k}|\sin(\theta/2) \tag{2.7}$$

and

$$\omega = N\Delta\nu, \tag{2.8}$$

where θ is the scattering angle between the two laser beams with absolute wavevector $|\boldsymbol{k}|$ and frequency difference $\Delta\nu$. Due to frequency difference $\Delta\nu$, there is a difference in the absolute wavevectors

$$\Delta|\boldsymbol{k}| = \frac{2\pi\Delta\nu}{c}, \tag{2.9}$$

where c is the speed of light $3 \cdot 10^8$ m/s. Thus the wavevector-difference is small and it may be omitted. For noninteracting atoms with the initial momentum $\hbar\boldsymbol{k}$, the Bragg condition is given by

$$\hbar\omega = \frac{q^2}{2m} + \frac{\hbar\boldsymbol{k}\cdot\boldsymbol{q}}{m}, \tag{2.10}$$

where the first term on rhs reflects the energy of a free particle and the second term is the Doppler shift.

The process described above may be used to probe the density fluctuations of the system and thus to directly measure the dynamic structure factor $S(\boldsymbol{k},\omega)$. The $S(\boldsymbol{k},\omega)$ is an essential property of the many-body quantum system allowing for comparison of theory and experiments. The measurement of $S(\boldsymbol{k},\omega)$ of the atomic gas in an optical trap is performed by pulsing on the laser light shortly before switching off the trap and determining the number of the scattered atoms as a function of the frequency difference $\Delta\nu$ between the laser beams. The measurements with different momentum transfers are carried out by changing the angle θ between the laser beam and the order N of the Bragg transition. Thus the Bragg scattering enables measurements of $S(\boldsymbol{k},\omega)$ over a wide range of parameters.

Instead of the Bragg-scattering, one could measure $S(\boldsymbol{k},\omega)$ using inelastic neutron scattering as in superfluid helium [57], or inelastic light scattering [34]. In contrast to measurements with any inelastic scattering, the Bragg scattering as described here is a stimulated process which greatly enhances the resolution and the sensitivity. The use of inelastic light scattering to determine $S(\boldsymbol{k},\omega)$

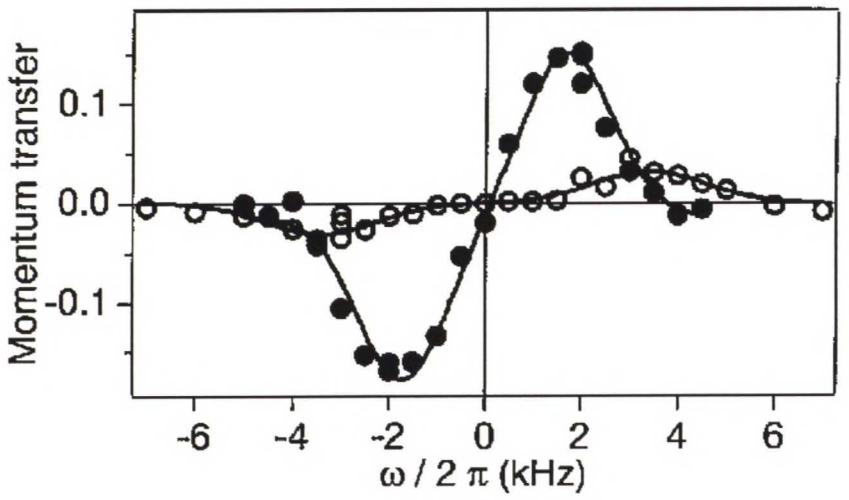

Figure 2.9: Bragg scattering from phonons and free particles. Momentum transfer per particle, in units of $\hbar k$, is shown vs the frequency difference between the laser beams. The open symbols present the phonon excitation in a trapped condensate and the closed symbols indicate the response of free particles after the trap is released. Graph from Ref. [21].

of a BEC would require the analysis of scattered light with kHz resolution and suffers from a strong background of coherently scattered light [49]. The Bragg diffraction is a background-free process in which the momentum transfer and the energy are predetermined by the laser beams, rather than postdetermined by the measurements of the momentum and energy of the scattered particle.

Bragg diffraction is a versatile technique for the manipulation of coherent matter waves. Using it, one can manipulate a BEC in a trap, and create multiple coherent components whose interaction and interference can be studied. It will be useful as an output coupler for an atom laser [10] since the large momentum transfer produces a directed output beam and the process is coherent. For the fermions, such coherent manipulation experiments have not been reported yet, but they are possible in principle [43].

3 Linear response theory

Any experiment conducted on a physical system involves the excitation of the system by some external probe, and the subsequent measurement of the system's response to that probe. If the interaction between the probe and the system is sufficiently weak, the system's response is linear. It is determined entirely by the properties of the system in the absence of the probe. The general theory of linear response [56] is applicable to both microscopic and macroscopic phenomena; it formulates the connections between the response and correlation functions, and the spectrum of elementary excitations. The theory provides a number of exact results of great practical importance.

3.1 Basic concepts

3.1.1 Second quantization

We denote a wavefunction of the many-body quantum system, a Fock state, using the occupation number representation

$$|\Phi\rangle = |n_1\, n_2 \ldots n_k \ldots n_\infty\rangle \equiv |n_1\rangle \otimes |n_2\rangle \otimes \cdots \otimes |n_\infty\rangle, \tag{3.1}$$

where $|n_k\rangle$ are the single-particle quantum states, and n_k are their occupation numbers. In Eq. (3.1), the index k refers to the kth lowest-energy state of the system with momentum $\boldsymbol{p}_k$. Let us suppose that $\boldsymbol{p}_k \neq \boldsymbol{p}_j$ for $k \neq j$. Thus we may express the Fock state as the product of momentum states

$$|\Phi\rangle = \bigotimes_{\boldsymbol{p}} |n_{\boldsymbol{p}}\rangle. \tag{3.2}$$

The states $|n_{\boldsymbol{p}}\rangle$ are orthonormal and they span a complete Hilbert space. By introducing the creation and annihilation operators $a_{\boldsymbol{p}}^{\dagger}$ and $a_{\boldsymbol{p}}$ we may write

$$|\Phi\rangle = \prod_{\boldsymbol{p}} \frac{1}{\sqrt{n_{\boldsymbol{p}}!}} \left(a_{\boldsymbol{p}}^{\dagger}\right)^{n_{\boldsymbol{p}}} \Big|0\Big\rangle, \tag{3.3}$$

where we denote the vacuum state of the system by $|0\rangle$. The creation and annihilation operators satisfy different algebras for bosons and fermions. For the bosons, they obey the commutation relations

$$\begin{aligned}
\left[\alpha_{\boldsymbol{p}}, \alpha_{\boldsymbol{p}'}^{\dagger}\right] &= \delta_{\boldsymbol{p},\boldsymbol{p}'} && (3.4)\\
\left[\alpha_{\boldsymbol{p}}, \alpha_{\boldsymbol{p}'}\right] &= 0 && (3.5)\\
\left[\alpha_{\boldsymbol{p}}^{\dagger}, \alpha_{\boldsymbol{p}'}^{\dagger}\right] &= 0 && (3.6)\\
\exists|0\rangle \quad \alpha_{\boldsymbol{p}}|0\rangle &= 0 \qquad \forall \boldsymbol{p}. && (3.7)
\end{aligned}$$

For the fermions they fullfill anticommutation relations

$$\begin{aligned}
\left\{\alpha_{\boldsymbol{p}}, \alpha_{\boldsymbol{p}'}^{\dagger}\right\} &= \delta_{\boldsymbol{p},\boldsymbol{p}'} && (3.8)\\
\left\{\alpha_{\boldsymbol{p}}, \alpha_{\boldsymbol{p}'}\right\} &= 0 && (3.9)\\
\left\{\alpha_{\boldsymbol{p}}^{\dagger}, \alpha_{\boldsymbol{p}'}^{\dagger}\right\} &= 0 && (3.10)\\
\exists|0\rangle \quad \alpha_{\boldsymbol{p}}|0\rangle &= 0 \qquad \forall \boldsymbol{p}. && (3.11)
\end{aligned}$$

For the free particles, one may write the annihilation operator

$$\rho_{\boldsymbol{p}} = \sum_{j} e^{i\boldsymbol{p}\cdot\boldsymbol{r}_j}. \tag{3.12}$$

When acting on $|0\rangle$, the operator

$$\rho_{\boldsymbol{q}}^{\dagger} = \sum_{\boldsymbol{p}} a_{\boldsymbol{p}+\boldsymbol{q}}^{\dagger} a_{\boldsymbol{p}} \tag{3.13}$$

produces single-particle transitions in which a given particle is scattered from the momentum state $\boldsymbol{p}$ to the state $\boldsymbol{p}+\boldsymbol{q}$.

Using creation and annihilator operators the ensemble average of the number operator is obtained through

$$n_{\boldsymbol{p}} = \langle a_{\boldsymbol{p}}^{\dagger} a_{\boldsymbol{p}} \rangle. \tag{3.14}$$

In addition, it follows from the above commutation relations (3.4–3.11) that

$$\alpha_{\boldsymbol{p}}^{\dagger}|n_{\boldsymbol{p}}\rangle = \sqrt{1 \pm n_{\boldsymbol{p}}}\,|n_{\boldsymbol{p}}+1\rangle, \tag{3.15}$$

where the $+$ $(-)$ sign stands for bosons (fermions).

3.1.2 Fermi's Golden Rule

According to the Fermi Golden Rule, the probability for a system in the initial state $|\Phi_0\rangle$ to absorb momentum $\boldsymbol{p}$ and energy ω is given by

$$p(\boldsymbol{p},\omega) = 2\pi|V_{\boldsymbol{p}}|^2 \sum_n |\langle\Phi_n|\,\rho^\dagger_{\boldsymbol{p}}\,|\Phi_0\rangle|^2 \delta(\omega_0+\omega-\omega_n), \tag{3.16}$$

where $V_{\boldsymbol{p}}$ is the amplitude of the perturbing field, $|\Phi_n\rangle$ are the eigenstates of the system, and ω_0 is the energy of the state $|\Phi_0\rangle$. Assuming nondegenerate energy levels and by using the result (3.15), one may rewrite Eq. (3.16) in the form

$$p(\boldsymbol{p},\omega) = 2\pi|V_{\boldsymbol{p}}|^2 n_0(1\pm n_{\boldsymbol{p}})\,\delta(\omega_0+\omega-\omega_{\boldsymbol{p}}), \tag{3.17}$$

where the upper sign stands for bosons and the lower one for fermions. The scattering process, depending on the occupation number of the final state, is enhanced or suppressed in Bose and Fermi gases, respectively. These effects are called bosonic stimulation and the Pauli exclusion principle.

In deriving the Fermi Golden Rule, one uses the first Born approximation for the scattering of light or particles by a system of interacting particles using density distribution functions. This is known to be valid if the system is in a pure quantum state and if this state does not change in the scattering process [6]. If the energy transfers occurring in the scattering process are negligible in comparison to the energy of the scattered photon or particle, the momentum transfer is essentially unique for each scattering angle.

We may express the rate of momentum transfer from system 1 to system 2 in the form

$$\frac{d\boldsymbol{P}_1}{dt} = \sum_{\boldsymbol{k}} \boldsymbol{k} \sum_{\omega} p_1(\boldsymbol{p},\omega)p_2(-\boldsymbol{p},-\omega) \tag{3.18}$$

$$= \sum_{\boldsymbol{k},\boldsymbol{q},\boldsymbol{p}} \boldsymbol{k}\; n_{\boldsymbol{p}}(1\pm n_{\boldsymbol{p}+\boldsymbol{k}})\, f_{\boldsymbol{q}}(1\pm f_{\boldsymbol{q}-\boldsymbol{k}})\,\delta(\omega_{\boldsymbol{p}+\boldsymbol{k}}-\omega_{\boldsymbol{p}}+\omega_{\boldsymbol{q}-\boldsymbol{k}}-\omega_{\boldsymbol{q}}), \tag{3.19}$$

where we denote the total momentum of system 1 by $\boldsymbol{P}_1$ and the distribution function for the system 2 by $f_{\boldsymbol{p}}$. By introducing the matrix elements $M_{\boldsymbol{p}}$, we take into account the presence of multi-particle processes, see Fig. 3.1. In this work we assume that $M_{\boldsymbol{p}}$ is function of momentum exchange $\boldsymbol{p}$ only. In general, it may be a function of energy ω, too. Substituting the matrix element and symmetrizing the notation for momentum, we obtain for the rate of momentum transfer

$$\frac{d\boldsymbol{P}_1}{dt} = \sum_{\substack{\boldsymbol{p}\,\boldsymbol{p}'\\ \boldsymbol{q}\,\boldsymbol{q}'}} (\boldsymbol{p}'-\boldsymbol{p})\; n_{\boldsymbol{p}}(1\pm n_{\boldsymbol{p}'})\;|M_{\boldsymbol{p}-\boldsymbol{p}'}|^2\; f_{\boldsymbol{q}}(1\pm f_{\boldsymbol{q}'})$$

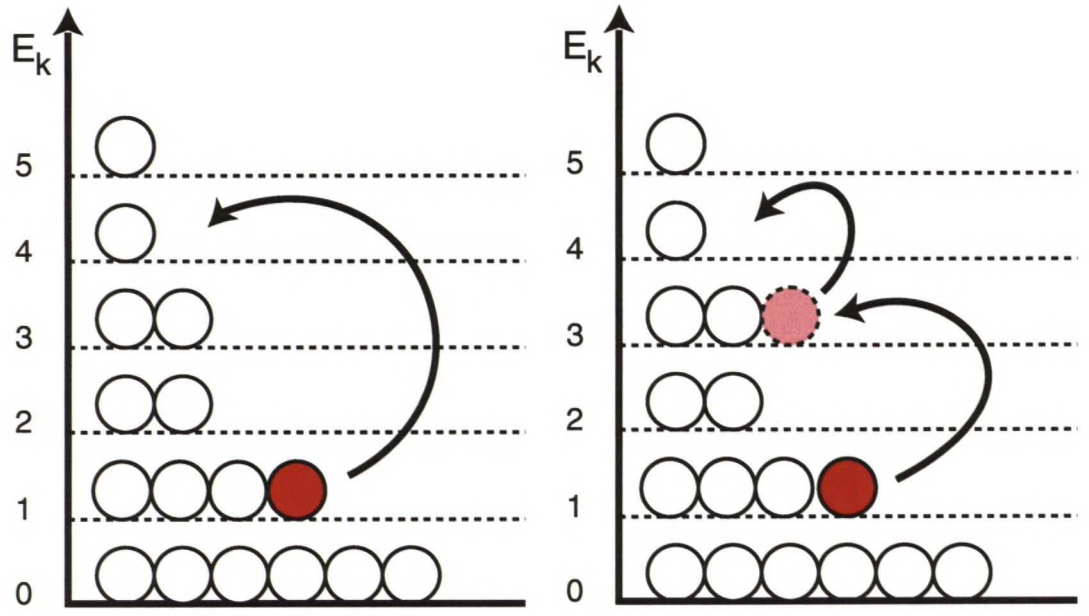

(a) Absorption of energy by a single particle.

(b) Energy absorption by two particles.

Figure 3.1: Energy level diagrams of two essentially different absorption processes.

$$\times\ (2\pi)^4\,\delta(\boldsymbol{p}+\boldsymbol{q}-\boldsymbol{p}'-\boldsymbol{q}')\,\delta(\omega_{\boldsymbol{p}}+\omega_{\boldsymbol{q}}-\omega_{\boldsymbol{p}'}-\omega_{\boldsymbol{q}'}), \qquad (3.20)$$

where $\boldsymbol{p}$, $\boldsymbol{p}'$, $\omega_{\boldsymbol{p}}$ and $\omega_{\boldsymbol{p}'}$ are the single-particle momenta and energies for system 1 before and after the collision. Above, $\boldsymbol{q}$, $\boldsymbol{q}'$, $\omega_{\boldsymbol{q}}$ and $\omega_{\boldsymbol{q}'}$ denote the same quantities for system 2. Symbols $n_{\boldsymbol{p}}$ and $f_{\boldsymbol{q}}$ denote the distribution functions for the systems 1 and 2, respectively.

3.1.3 Elementary excitations

In an interacting quantum gas, the elementary excitations may be pictured as noninteracting quasiparticles [56], in close analogy with the single-particle excitations of a noninteracting gas. In an interacting Fermi system, the quasiparticles are particle-like states above the Fermi surface and hole-like ones below the Fermi energy. In an interacting BEC, one has Bogoliubov quasiparticles, which are superpositions of the free-particle momentum states $+\boldsymbol{q}$ and $-\boldsymbol{q}$. Here we assume noninteracting quasiparticles, in other words, their lifetime is infinite. Consequently, the eigenstates are well defined. However, it is hard to

excite noninteracting quasiparticles. Thus we allow all the processes to happen adiabatically slowly. The system then remains in thermal equilibrium and the distribution of quasiparticles may be characterized by the distribution function $n_{\boldsymbol{p}}$. The excitation of the system is measured through the deviation $\delta n_{\boldsymbol{p}}$ from the ground-state distribution $n^0_{\boldsymbol{p}}$

$$\delta n_{\boldsymbol{p}} = n_{\boldsymbol{p}} - n^0_{\boldsymbol{p}}. \tag{3.21}$$

Let us assume the deviations $\delta n_{\boldsymbol{p}}$ to be small and to contain only long-wavelength fluctuations, such that we may calculate the values of the physical quantities from the linear terms in a Taylor expansion. Let us emphasize that the single-particle theories are not complete. There exist many-body effects that arise as a consequence of quasiparticle interactions that are characteristic to some systems, but we need not consider these effects in what follows.

3.1.4 Mobility

Here we consider the mobility of the charged impurities, say ions, in the gas. In the absence of an external electric field $\mathcal{E}$, the particles undergo Brownian motion. The time evolution of the density of the impurity particles ρ is governed by the diffusion equation

$$\frac{\partial \rho}{\partial t} = D\nabla\rho. \tag{3.22}$$

Einstein's relation defines the mobility

$$\mu = eD/k_{\mathrm{B}}T. \tag{3.23}$$

The Langevin theory [55] of Brownian motion suggests for the momentum transfer rate of the impurity

$$\frac{d\boldsymbol{P}}{dt} = \mathfrak{F}(t), \tag{3.24}$$

where

$$\mathfrak{F}(t) = -\frac{\boldsymbol{v}}{\mu} + e\mathcal{E} + \mathcal{F}(t). \tag{3.25}$$

Above, in the first friction-like term, $\boldsymbol{v}$ is the velocity of the impurity with respect to the gas, and μ is called mobility, e is the charge of the impurity and $\mathcal{E}$ is the electric field. Finally the last term is a rapidly oscillating force $\mathcal{F}(t)$ due to collisions with the gas atoms which satisfies

$$\bar{\mathcal{F}}(t) = 0. \tag{3.26}$$

Substituting $\mathcal{E} = 0$ and taking the ensemble average of Eq. (3.25), one obtains

$$\frac{d\langle \boldsymbol{P} \rangle}{dt} = \frac{\langle \boldsymbol{v} \rangle}{\mu}, \tag{3.27}$$

which establishes the connection of the mobility to measurable quantities. The relaxation time τ is related to the mobility via

$$\tau = \frac{\mu}{m}, \tag{3.28}$$

where m is the mass of the impurity.

Let us now discuss the motion of charged impurities when an electric field $\mathcal{E}$ is applied. In general, we must calculate the mobility using the nonequilibrium distribution function $n_{\boldsymbol{p}}$. Here we assume that the distribution function $n_{\boldsymbol{p}}$ is close to the equilibrium distribution function $n^0_{\boldsymbol{p}}$ and express it using the Taylor series. The linear terms of the Taylor series of $n_{\boldsymbol{p}}$ are known as the Boltzmann equation

$$n_{\boldsymbol{p}} = n^0_{\boldsymbol{p}} + \mu \mathcal{E} e \cdot \nabla_{\boldsymbol{p}} n^0_{\boldsymbol{p}}, \tag{3.29}$$

where μ is the mobility and $\mathcal{E}$ is the electric field.

3.2 Linear response functions

The response of a system to an external probe is closely linked with the correlations which exist between the positions and momenta of the particles. The dynamic structure factor, $S(\boldsymbol{k}, \omega)$, represents the maximum information one can obtain about the system's behavior in scattering experiments. Some theoretical studies are based on the density-density response function, the generalized susceptibility $\chi(\boldsymbol{k}, \omega)$. When the particle-like properties are dominant, the scattering cross-section $d\sigma/d\Omega$ is an important quantity. The quantities listed above are all linear response functions and the relationships between them are described below.

3.2.1 Dynamic structure factor

The dynamic structure factor (van Hove, structure- or scattering function) of a many-body system is defined in Ref. [56] as the Fourier transform of the density-density correlation function

$$S(\boldsymbol{k},\omega) = \frac{1}{\mathcal{Z}} \sum_{m\,n} e^{-\beta E_m} |\langle m|\rho_{\boldsymbol{k}}|n\rangle|^2 \, \delta(\omega - \omega_m - \omega_n), \tag{3.30}$$

where $\boldsymbol{k}$ and ω are the momentum and energy transferred by the probe to the sample. Here $|n\rangle$ and E_n are the eigenstates and eigenvalues of the Hamiltonian of the system. We denote the annihilation operator associated with momentum $\boldsymbol{k}$ by $\rho_{\boldsymbol{k}}$ and $\mathcal{Z}$ stands for the canonical partition function.

Defined as above, $S(\boldsymbol{k},\omega)$ describes the way in which a system of N particles (linearly) responds to a probe which produces a density fluctuation described by the operator $\rho_{\boldsymbol{k}}$. The response is independent of the mass and energy of the scattered particle as well as of the interaction potential.

The definition (3.30) yields the following consequence

$$S(\boldsymbol{k},\omega) = S(-\boldsymbol{k},\omega), \tag{3.31}$$

which may be interpreted as the invariance of the system's response under the time reversal. The relationship

$$S(\boldsymbol{k},\omega) = e^{\beta\omega} S(\boldsymbol{k},-\omega) \tag{3.32}$$

known as the principle of detailed balance [56] gives the rate of energy transfer from the system to the probe, and vice versa.

Moreover, by imposing particle conservation, we obtain

$$\int_{-\infty}^{\infty} d\omega\, \omega S(\boldsymbol{k},\omega) = \frac{Nk^2}{m}, \tag{3.33}$$

where m is the particle mass and N is the total number of particles in the system. The relation (3.33) is known as the f-sum rule.

In the long-wavelength limit, $S(\boldsymbol{k},\omega)$ is related to the compressibility κ of the system, and one obtains the compressibility sum rule

$$\lim_{\boldsymbol{k}\to 0} \left[\int_{-\infty}^{\infty} d\omega \, \frac{S(\boldsymbol{k},\omega)}{\omega} \right] = \frac{N}{ms^2}, \tag{3.34}$$

where $s = (\kappa m \rho)^{-1/2}$ is the isothermal sound velocity and m is the particle mass and the mass density is denoted by ρ.

Let us consider an infinite, isotropic, noninteracting gas. The Hamiltonian for the system may be written as

$$H = \sum_{p} \frac{\boldsymbol{p}^2}{2m} a_{\boldsymbol{p}}^{\dagger} a_{\boldsymbol{p}}, \tag{3.35}$$

where the $a_{\boldsymbol{p}}^{\dagger}$ and $a_{\boldsymbol{p}}$ are the creation and annihilation operators of particles with momentum $\boldsymbol{p}$. The particle mass is denoted by m. For free particles, the creation and annihilation operators may be written as $a_{\boldsymbol{p}} = e^{i\boldsymbol{p}\cdot\boldsymbol{r}}$ and $a_{\boldsymbol{p}}^{\dagger} = e^{-i\boldsymbol{p}\cdot\boldsymbol{r}}$.

Consequently, the orthogonality of the eigenstates $|n\rangle = e^{i\boldsymbol{k}_n\cdot\boldsymbol{r}}$ leads to momentum conservation

$$|\langle m|\rho_{\boldsymbol{k}}|n\rangle|^2 = |C_{mn}|^2\,\delta(\boldsymbol{p}_n + \boldsymbol{k} + \boldsymbol{p}_m), \tag{3.36}$$

where $\boldsymbol{p}_j$ is the momentum associated with state $|j\,\rangle$. The possibility for a single particle to occupy the energy level E_i may be expressed as

$$\frac{e^{-\beta E_i}}{\mathcal{Z}} = \frac{n_{\boldsymbol{p}}}{N}, \tag{3.37}$$

where $\mathcal{Z}$ stands for the canonical partition function, $n_{\boldsymbol{p}}$ is the distribution function and N is the total number of particles in the system.

Using the above reasoning, one may rewrite Eq. (3.30) in the useful form

$$S(\boldsymbol{k},\omega) = |C_{\boldsymbol{k}}|^2 \sum_{\boldsymbol{p},\boldsymbol{p}'} n_{\boldsymbol{p}}(1 \pm n_{\boldsymbol{p}'})\,\delta(\boldsymbol{p} + \boldsymbol{k} - \boldsymbol{p}')\,\delta(\omega_{\boldsymbol{p}} + \omega - \omega_{\boldsymbol{p}'}). \tag{3.38}$$

The dynamical structure factor contains distinct quantum-statistical features in the case of fermionic and bosonic atomic gases. For a Fermi gas it demonstrates the Fermi inhibition of the spontaneous scattering of photons [27, 35]. Transfer of momenta comparable to or less than the Fermi momentum is excluded due to the occupation of the possible final states. This leads to a suppression of the long-wavelength response in a degenerate Fermi gas. For a Bose gas, $S(\boldsymbol{k},\omega)$ reflects bosonic enhancement [22]. In this case, the occupation of the final state enhances the momentum transfer. The allowed excitations are illustrated in Figs. 3.2 as functions of the momentum transfer .

3.2.2 Static structure factor

Let us define the static structure factor as

$$S(\boldsymbol{k}) = \frac{1}{N}\int_0^{\infty} d\omega S(\boldsymbol{k},\omega), \tag{3.39}$$

where N is the number of particles in the system. The static structure factor is a useful quantity when the system is probed using high-velocity particles that sample the density correlations over a time scale which is much shorter than the characteristic periods in the system.

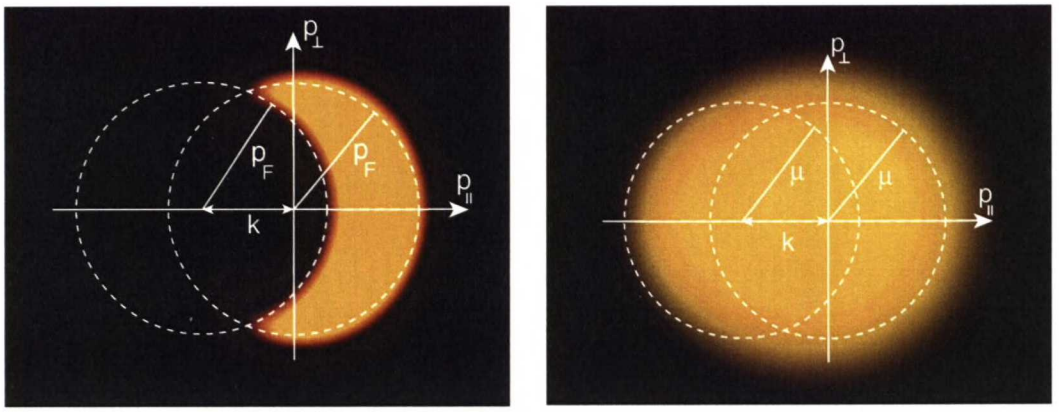

(a) Fermi system.

(b) Bose system.

Figure 3.2: Yellow areas represent the allowed excitations in a quantum gas when probed with particles of momentum $\boldsymbol{k}$.

3.2.3 Generalized susceptibility

The theoretical considerations on the response of the system to density fluctuations may be more straightforward using the an analytic density-density response function

$$\chi(\boldsymbol{k},\omega) = \frac{\langle \rho(\boldsymbol{k},\omega)\rangle}{\varphi(\boldsymbol{k},\omega)} \tag{3.40}$$

where $\varphi(\boldsymbol{k},\omega)$ is the Fourier transform of the scalar potential $\varphi(\boldsymbol{r},\omega)$ which acts on the system and $\langle \rho(\boldsymbol{k},\omega)\rangle$ stands for the average density fluctuation induced by the perturbation. When the probe potential is weak, one may use first-order perturbation theory and rewrite Eq. (3.40) in the form

$$\chi(\boldsymbol{k},\omega) = \sum_n |\langle n|\rho_{\boldsymbol{k}}|0\rangle|^2 \frac{2(\omega_n-\omega_0)}{(\omega+i\eta)^2-(\omega_n-\omega_0)^2}, \tag{3.41}$$

where ω_n is the energy of the state $|n\rangle$. In Eq. (3.41), a small positive infinitesimal quantity η, representing dissipation, is introduced to avoid mathematical singularities. The one-to-one relationship between $\chi(\boldsymbol{k},\omega)$ and $S(\boldsymbol{k},\omega)$ is known

as the fluctuation-dissipation theorem [56]

$$S(\boldsymbol{k},\omega) = \frac{\chi''(\boldsymbol{k},\omega)}{\pi\left(e^{-\beta\omega}-1\right)}, \tag{3.42}$$

where $\chi''(\boldsymbol{k},\omega)$ is the imaginary, absorptive (since $\omega\chi(\boldsymbol{k},\omega)$ represents energy dissipation), part of $\chi(\boldsymbol{k},\omega)$.

3.2.4 Scattering cross-section

The differential scattering cross-section $d\rho/d\Omega$ is obtained from $S(\boldsymbol{k},\omega)$ using the Born approximation [6]

$$\frac{d\sigma}{d\Omega} = \frac{m^2}{4\pi^2\hbar^5}\frac{k}{k_0}W(\boldsymbol{k})\int S(\boldsymbol{k},\omega)\,d\omega, \tag{3.43}$$

where the Fourier transform of the interaction potential $V(\boldsymbol{r})$ is denoted by $W(\boldsymbol{k}) = \left(\int e^{i\boldsymbol{k}\cdot\boldsymbol{r}}V(\boldsymbol{r})d\boldsymbol{r}\right)^2$. Above m, k, and k_0 are the mass, and the initial and final wave vectors of the scattered particle.

3.3 Linear response of dilute gases

Let us first consider an integral that appears frequently in the following calculations of the dynamic structure factor. From mathematics, one knows that

$$\int_a^b f(x)\,\delta(g(x))\,dx = \int_a^b f(x)\sum_i \frac{\delta(x-x_i)}{|g'(x_i)|}dx \tag{3.44}$$

$$= \sum_i \frac{f(x_i)}{|g'(x_i)|}, \tag{3.45}$$

where $g(x_i) = 0$, $a \le x_i \le b$ with $\delta(x)$ denoting the Dirac delta function. Let us examine the following integral

$$\int d\boldsymbol{p} f(p)\,\delta(\omega+\omega_{\boldsymbol{p}}-\omega_{\boldsymbol{p}+\boldsymbol{k}}) = \int d\boldsymbol{p} f(p)\,\delta\left(\omega+\frac{\boldsymbol{p}^2}{2m}-\frac{(\boldsymbol{p}+\boldsymbol{k})^2}{2m}\right), \tag{3.46}$$

where we have assumed $\omega_p = p^2/2m$ for the momentum-energy dispersion relation. Introducing cylindrical coordinates and setting the z-axis parallel to $\boldsymbol{k}$, one

obtains

$$\int d\boldsymbol{p} f(p)\,\delta(\omega+\omega_{\boldsymbol{p}}-\omega_{\boldsymbol{p}+\boldsymbol{k}}) = \int dp_z f(p_z)\,\delta\left(\omega-\frac{p_z k}{m}-\frac{k^2}{2m}\right) \quad (3.47)$$

$$= \int dp_z f(p_z)\frac{\delta(p_z+\frac{m\omega}{k}-\frac{k}{2})}{|-k/m|} \quad (3.48)$$

$$= \frac{m}{k} f(\frac{k}{2}-\frac{m\omega}{k}). \quad (3.49)$$

The above result states the useful relationship between the value of the integral on the lhs of Eq. (3.47) and the magnitude k of the vector $\boldsymbol{k}$.

3.3.1 Classical gas

In thermal equilibrium, an ideal classical gas is described by the Maxwell-Boltzmann distribution

$$n_{\boldsymbol{p}} = e^{-\beta(p^2/2m-\mu)}, \quad (3.50)$$

where $\beta = k_{\mathrm{B}}T$ and μ is the chemical potential. Both Fermi and Bose statistics approach the classical distribution in the high-temperature limit. One may write Eq. (3.38) in the form

$$S(\boldsymbol{k},\omega) = \sum_{\boldsymbol{p}\boldsymbol{p}'} n_{\boldsymbol{p}}\,\delta(\boldsymbol{p}+\boldsymbol{k}-\boldsymbol{p}')\,\delta(\omega_{\boldsymbol{p}}+\omega-\omega_{\boldsymbol{p}'}) \quad (3.51)$$

$$= \sum_{\boldsymbol{p}} e^{-\beta(p^2/2m-\mu)}\,\delta\left(\omega+\frac{\boldsymbol{p}^2}{2m}-\frac{(\boldsymbol{p}+\boldsymbol{k})^2}{2m}\right) \quad (3.52)$$

$$\approx \int \frac{d\boldsymbol{p}}{(2\pi\hbar)^3} e^{-\beta(p^2/2m-\mu)}\,\delta\left(\omega+\frac{\boldsymbol{p}^2}{2m}-\frac{(\boldsymbol{p}+\boldsymbol{k})^2}{2m}\right). \quad (3.53)$$

Using the result in Eq. (3.49)

$$S(\boldsymbol{k},\omega) = \frac{m}{k}\frac{2\pi}{(2\pi\hbar)^3}\int_{-\infty}^{\infty} dp_z \int_0^{\infty} p_\perp dp_\perp\, e^{-\beta\left(\frac{p_z^2+p_\perp^2}{2m}-\mu\right)}\,\delta\left(p_z-\frac{\omega k}{m}-\frac{k}{2}\right) \quad (3.54)$$

$$= \frac{m}{k}\frac{2\pi}{(2\pi\hbar)^3}\int_0^{\infty} p_\perp dp_\perp\, e^{-\beta\left(p_\perp^2/2m+\left(\frac{\omega m}{k}-\frac{k}{2}\right)^2/2m-\mu\right)} \quad (3.55)$$

$$= \frac{m}{k}\frac{2\pi}{(2\pi\hbar)^3}\, e^{-\beta\left(\left(\frac{\omega m}{k}-\frac{k}{2}\right)^2/2m-\mu\right)}\int_0^{\infty} p_\perp dp_\perp\, e^{-\beta p_\perp^2/2m} \quad (3.56)$$

$$= \frac{m}{k}\frac{2\pi}{(2\pi\hbar)^3}\, e^{\beta\mu} e^{\frac{-\beta m}{2k^2}\left(\omega-\frac{k^2}{2m}\right)^2}\frac{m}{\beta} \quad (3.57)$$

$$= \frac{m^2}{\beta k}\frac{2\pi}{(2\pi\hbar)^3}\, e^{\beta\mu} e^{\frac{-\beta m}{2k^2}\left(\omega-\frac{k^2}{2m}\right)^2}. \quad (3.58)$$

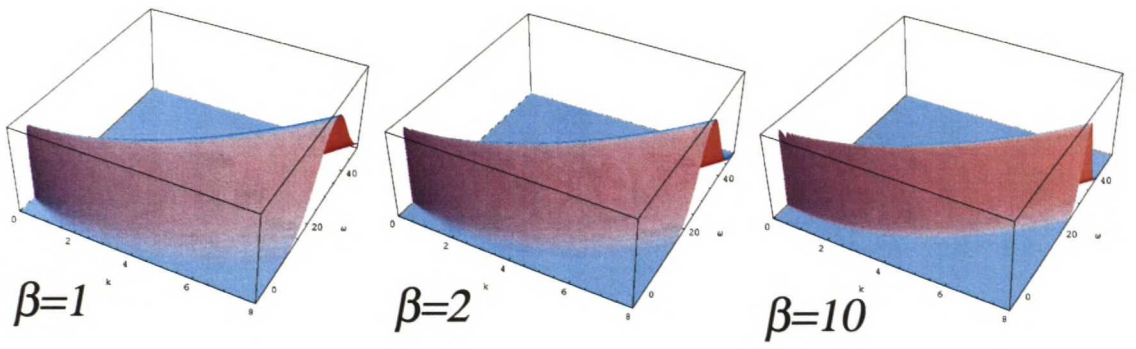

Figure 3.3: Temperature dependence of the dynamic structure factor for a classical Maxwell-Boltzmann gas.

The particle number in the system is obtained by integrating the distribution function

$$N = \int \frac{d^3\boldsymbol{p}}{(2\pi\hbar)^3} e^{-\beta p^2/2m} e^{\beta\mu} = \frac{1}{(2\pi\hbar)^3} \left(\frac{2\pi m}{\beta}\right)^{3/2} e^{\beta\mu}. \tag{3.59}$$

Consequently

$$S(\boldsymbol{k},\omega) = \frac{N}{k}\sqrt{\frac{m\beta}{2\pi}}\, e^{\frac{-\beta m}{2k^2}(\omega - \frac{k^2}{2m})^2}, \tag{3.60}$$

which is the dynamic structure factor of a classical gas.

3.3.2 Quantum gas

Here we calculate the general form of the dynamic structure factor for noninteracting quantum gases. In thermal equilibrium, an ideal quantum gas is described by the Bose (-) or Fermi (+) distribution function

$$n_{\boldsymbol{p}} = \frac{1}{e^{\beta(p^2/2m-\mu)} \pm 1}, \tag{3.61}$$

where μ represents the chemical potential for Bose particles and the Fermi energy for fermions. Substituting the general form of the distribution in Eq. (3.38) yields

$$S(\boldsymbol{k},\omega) = \sum_{\boldsymbol{p}\boldsymbol{p}'} n_{\boldsymbol{p}}(1 \pm n_{\boldsymbol{p}'})\, \delta(\boldsymbol{p}+\boldsymbol{k}-\boldsymbol{p}')\, \delta(\omega_{\boldsymbol{p}} + \omega - \omega_{\boldsymbol{p}'}) \tag{3.62}$$

$$\approx \int \frac{d\boldsymbol{p}}{(2\pi\hbar)^3} \delta\left(\omega + \frac{\boldsymbol{p}^2}{2m} - \frac{(\boldsymbol{p}+\boldsymbol{k})^2}{2m}\right) \times \frac{1}{e^{\beta(\epsilon_{\boldsymbol{p}}-\mu)} \pm 1} \left(1 \mp \frac{1}{e^{\beta(\epsilon_{\boldsymbol{p}+\boldsymbol{k}}-\mu)} \pm 1}\right). \tag{3.63}$$

By using the result in Eq. (3.49)

$$
\begin{aligned}
S(\boldsymbol{k},\omega) &= \frac{m}{k}\frac{2\pi}{(2\pi\hbar)^3}\int_{-\infty}^{\infty}dp_z\int_0^{\infty}p_\perp dp_\perp\,\delta\left(p_z-\frac{\omega k}{m}-\frac{k}{2}\right)\\
&\quad\times\frac{1}{e^{\beta(p_\perp^2/2m+p_z^2/2m-\mu)}\pm 1}\left(1\mp\frac{1}{e^{\beta(p_\perp^2/2m+(p_z+k)^2/2m-\mu)}\pm 1}\right) \qquad (3.64)\\
&= \frac{m}{k}\frac{2\pi}{(2\pi\hbar)^3}\frac{2m}{\beta}\int_0^{\infty}\sqrt{\frac{\beta}{2m}}p_\perp d\sqrt{\frac{\beta}{2m}}p_\perp\frac{1}{e^{\beta p_\perp^2/2m+(\omega m/k-k/2)^2/2m-\beta\mu}\pm 1}\\
&\quad\times\left(1\mp\frac{1}{e^{\beta p_\perp^2/2m+(\omega m/k-k/2)^2/2m-\beta\mu}\pm 1}\right) \qquad (3.65)\\
&= \frac{2m^2}{k\beta}\frac{2\pi}{(2\pi\hbar)^3}\frac{\mp 1}{2}\frac{1}{1-e^{-\beta\omega}}\ln\left[\frac{e^{\frac{\beta}{8mk^2}(k^2+2m\omega)^2-\beta\mu}\mp e^{\beta\omega}}{e^{\frac{\beta}{8mk^2}(k^2+2m\omega)^2-\beta\mu}\mp 1}\right] \qquad (3.66)\\
&= \frac{m^2}{k\beta}\frac{2\pi}{(2\pi\hbar)^3}\frac{\mp 1}{1-e^{-\beta\omega}}\ln\left[\frac{1\mp e^{\beta\omega}e^{-\frac{\beta}{8mk^2}(k^2+2m\omega)^2+\beta\mu}}{1\mp e^{-\frac{\beta}{8mk^2}(k^2+2m\omega)^2+\beta\mu}}\right] \qquad (3.67)\\
&= \frac{m^2}{k\beta}\frac{2\pi}{(2\pi\hbar)^3}\frac{\mp 1}{1-e^{-\beta\omega}}\ln\left[\frac{1\mp e^{-\frac{\beta}{8mk^2}(k^2+2m\omega)^2+\beta\mu}}{1\mp e^{-\frac{\beta}{8mk^2}(k^2-2m\omega)^2+\beta\mu}}\right], \qquad (3.68)
\end{aligned}
$$

where the upper signs hold for bosons and the lower ones for fermions.

For the Bose gas, we find that the integrand in Eq. (3.64) is not defined when $z=1$ and $\omega=k^2/2m$, which corresponds the contribution of the Bose-Einstein condensate

$$
S_0(\boldsymbol{k},\omega)=\frac{n_0}{1-e^{-\beta\omega}}\left[\delta(\omega-k^2/2m)-\delta(\omega-k^2/2m)\right]. \qquad (3.69)
$$

Let us introduce the dimensionless variables $\tilde{k}=k/k_0$, $\tilde{\omega}=\omega/\epsilon_0$, and $\tilde{T}=1/\beta\epsilon_0$, where $k_0=\rho^{1/3}$ and $\epsilon_0=k_0^2/2m$. Finally, we denote the fugacity by $z=e^{\mu/k_{\mathrm{B}}T}$. Using this new set of variables we may write Eq. (3.68) in the form

$$
\begin{aligned}
S(\boldsymbol{k},\omega) &= \frac{m\tilde{T}}{2\epsilon_0\tilde{k}}\frac{1}{1-e^{-\tilde{\omega}/\tilde{T}}}\ln\left[\frac{1-ze^{-(\tilde{k}+\tilde{\omega}/\tilde{k})^2/4\tilde{T}}}{1-ze^{-(\tilde{k}-\tilde{\omega}/\tilde{k})^2/4\tilde{T}}}\right]\\
&\quad+\frac{1}{1-e^{-\tilde{\omega}/\tilde{T}}}\left[\delta(\tilde{\omega}-\tilde{k}^2)-\delta(\tilde{\omega}-\tilde{k}^2)\right]. \qquad (3.70)
\end{aligned}
$$

For a Fermi gas, we introduce the dimensioless variables $\tilde{k}=k/k_{\mathrm{F}}$, $\tilde{\omega}=\omega/\epsilon_{\mathrm{F}}$, and $\tilde{T}=1/\beta\epsilon_{\mathrm{F}}$, where k_F is the Fermi energy and $\epsilon_{\mathrm{F}}=k_{\mathrm{F}}^2/2m$. Above, μ is defined to be the Fermi energy ϵ_{F}. Using this new set of variables we may write

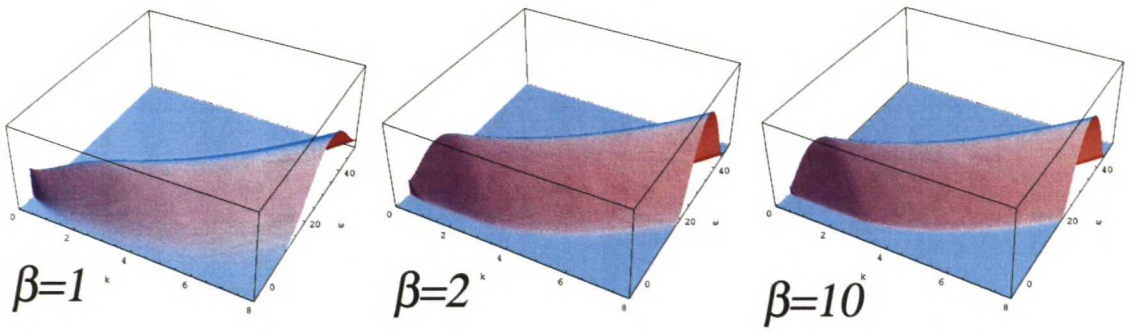

Figure 3.4: Temperature dependence of the dynamic structure factor for a non-interacting Fermi gas.

Eq. (3.68)

$$S(\boldsymbol{k},\omega) = \frac{m\tilde{T}}{2\epsilon_0 \tilde{k}} \frac{2\pi}{1-e^{-\tilde{\omega}/\tilde{T}}} \ln\left[\frac{1+e^{-(\tilde{k}-\tilde{\omega}/\tilde{k})^2/4\tilde{T}+1/\tilde{T}}}{1+e^{-(\tilde{k}+\tilde{\omega}/\tilde{k})^2/4\tilde{T}+1/\tilde{T}}}\right], \tag{3.71}$$

which is the dynamic structure factor for a Fermi gas. The above results are similar to those obtained in Refs. [35, 58, 60, 61] using the generalized susceptibility.

3.3.3 Internal interactions

In the interacting system, density fluctuations may be formed of single quasiparticles of momentum $\boldsymbol{q}$. There will be, in addition, contributions to the excitation spectrum from multiparticle configurations, involving two or more quasiparticles, of total momentum $\boldsymbol{q}$.

Let us consider the contribution $S^{(n)}(\boldsymbol{q},\omega)$ arising from the excitations of several quasiparticle-quasihole pairs. For the interacting system, the density fluctuation $\rho_{\boldsymbol{q}}^{\dagger}$ may couple such multiparticle configurations to the ground state. Since momentum conservation involves only the total momentum, there is essentially no limitation on the momentum of any single quasiparticle in such configurations. The multiparticle excitation energy will therefore vary over a broad range. The corresponding contribution $S^{(n)}(\boldsymbol{q},\omega)$ has no particular structure and it will appear as a broad background. For a Fermi system at low energies one can show, using the exclusion principle, that $S^{(n)}(\boldsymbol{q},\omega)$ vanishes as ω^3. It is negligible compared to the single-pair contribution, which is of order ω. The structure factor for an interacting Fermi gas is sketched in Fig. 3.5.

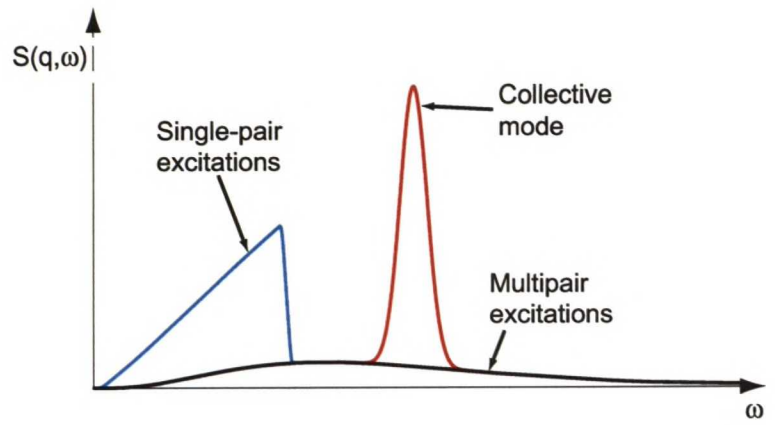

Figure 3.5: Dynamic structure factor for an interacting Fermi gas when $\boldsymbol{q} \to 0$. The phonons give a peaked contribution to $S(\boldsymbol{q}, \omega)$, whereas the multiparticle excitations are seen as the broad background.

The structure factor for a system with single-particle internal interactions may be described by

$$S_{\text{int}}(\boldsymbol{q}, \omega) = S_{\text{non-int}}(\boldsymbol{q}, \omega) + S^{(1)}(\boldsymbol{q}, \omega). \tag{3.72}$$

The first term on the right-hand side represents a contribution from single-particle excitations. The second is the contribution from configurations involving two or more quasiparticles. An expression of the form in Eq. (3.72) will present a reasonable approximation for the structure factor when the lifetime of the quasiparticles is sufficiently long [57].

In the interacting Fermi gas, the effect of the formation of the quasiparticle-quasihole pairs may be described by a phonon spectrum [56].

$$S(\boldsymbol{q}, \omega) = S_{\text{non-int}}(\boldsymbol{q}, \omega) + d_{\boldsymbol{q}} \left[(n_{\boldsymbol{q}} + 1)\delta(\omega - \omega_{\boldsymbol{q}}) + n_{\boldsymbol{q}}\delta(\omega + \omega_{\boldsymbol{q}}) \right], \tag{3.73}$$

where $d_{\boldsymbol{q}}$ is the constant depending of the strength of the interaction.

The excited states of an interacting BEC may be approximated with the Bogoliubov spectrum [21]

$$(\hbar\omega)^2 = \left(\frac{\hbar^2 q^2}{2m} \right) \left(\frac{\hbar^2 q^2}{2m} + 2gn \right), \tag{3.74}$$

where the coupling constant g is related to the scattering length $a = gm/4\pi\hbar$. In Eq. (3.74), we denote the wavevector of the excitations by $\boldsymbol{q}$. For large momenta, the spectrum coincides with the free-particle energy

$$\hbar\omega = \frac{\hbar^2 q^2}{2m}. \tag{3.75}$$

For low momenta, Eq. (3.74) instead reduces to the phonon dispersion relation

$$\omega = cq, \tag{3.76}$$

where $c = \sqrt{gn/m}$ is the sound velocity. The transition between the two regimes occurs when the typical wavelength of the excited states becomes on the order of the healing length

$$\xi = \sqrt{8\pi na}, \tag{3.77}$$

which is an important length scale for superfluidity.

3.4 Some special cases

Above, we have derived a general formula for the structure factor for ideal quantum and classical gases. Below we evaluate $S(\boldsymbol{k}, \omega)$ in the some limits. The expressions obtained for $S(\boldsymbol{k}, \omega)$ are more useful and employed for further studies in the next Chapter.

3.4.1 Heavy impurity

When considering heavy impurity particles moving in a quantum gas, it is a fair approximation to regard them as recoilless particles. First, consider the structure factor for fast moving impurities. We may assume them to be as classical particles. Let us evaluate the structure factor in the heavy-particle limit

$$S(\boldsymbol{k}, \omega) = \lim_{m\to\infty} \frac{N}{k}\sqrt{\frac{m\beta}{2\pi}}\, e^{\frac{-\beta m}{2k^2}(\omega - \frac{k^2}{2m})^2}. \tag{3.78}$$

The integration of $S(\boldsymbol{k}, \omega)$ over ω yields

$$\int_{-\infty}^{\infty} d\omega \frac{N}{k}\sqrt{\frac{m\beta}{2\pi}}\, e^{\frac{-\beta m}{2k^2}(\omega - \frac{k^2}{2m})^2} = N. \tag{3.79}$$

On the other hand, for $\omega \neq \frac{k^2}{2m}$

$$\lim_{m\to\infty} \frac{N}{k}\sqrt{\frac{m\beta}{2\pi}}\, e^{\frac{-\beta m}{2k^2}(\omega - \frac{k^2}{2m})^2} = \lim_{m\to\infty} \frac{N}{k}\sqrt{\frac{m\beta}{2\pi}}\, e^{\frac{-\beta m\omega^2}{2k^2}} = 0. \tag{3.80}$$

Thus, combining Eqs. (3.79) and (3.80), we obtain

$$S(\boldsymbol{k}, \omega) = N\delta\left(\omega - \frac{k^2}{2m}\right), \tag{3.81}$$

where N is the total number of impurity particles.

In the diffusive limit, impurity motion is governed by the relaxation equation

$$m\frac{\partial \boldsymbol{j}}{\partial t} + \nabla P = -m\frac{\boldsymbol{j}}{\tau}, \tag{3.82}$$

where $\boldsymbol{j}$ is the impurity current, $P = \rho k_{\mathrm{B}} T$ is the effective pressure, and $\tau = \mu/m$ is the relaxation time, where μ is the mobility. From the Fourier transform of Eq. (3.82) and the continuity equation

$$\frac{d\boldsymbol{j}}{dt} + \nabla \cdot \boldsymbol{j} = 0 \tag{3.83}$$

one may calculate [62] the generalized susceptibility

$$\chi(\boldsymbol{k}, \omega) = -2\pi \frac{Nk^2}{M\omega(\omega + i/\tau) - k^2 k_{\mathrm{B}} T}. \tag{3.84}$$

Finally, using the fluctuation-dissipation theorem Eq. (3.42) and Einstein's relation, Eq. (3.23), one obtains

$$S(\boldsymbol{k}, \omega) = \frac{\beta\omega}{1 - e^{-\beta\omega}} \frac{2NDk^2}{\omega^2 + (Dk^2 - \omega^2\tau)^2}. \tag{3.85}$$

Thus, in the diffusive limit, the scattering of the impurities results in a diffusive peak at $\omega = 0$ with width Dk^2 instead of the free particle peak at $\omega = k^2/2m$ in Eq. (3.81).

3.4.2 Non-degenerate system

Here we evaluate the high-temperature limit of the structure factor for a quantum gas. The contribution of ground-state atoms may be negleted, since $z \to 0$ as the temperature increases. Let us rewrite Eq. (3.68)

$$S(\boldsymbol{k}, \omega) = \pm \frac{m\tilde{T}}{2\epsilon_0 \tilde{k}} \frac{2\pi}{1 - e^{-\tilde{\omega}/\tilde{T}}} \ln\left[\frac{1 \mp z e^{-(\tilde{k} + \tilde{\omega}/\tilde{k})^2/4\tilde{T}}}{1 \mp z e^{-(\tilde{k} - \tilde{\omega}/\tilde{k})^2/4\tilde{T}}}\right], \tag{3.86}$$

In the high-temperature limit, Eq. (3.86) reduces to

$$S(\boldsymbol{k}, \omega) = \pm \frac{m\tilde{T}}{2\epsilon_0 \tilde{k}} \frac{2\pi}{1 - e^{-\tilde{\omega}/\tilde{T}}} (\mp z e^{-(\tilde{k} + \tilde{\omega}/\tilde{k})^2/4\tilde{T}} \pm z e^{-(\tilde{k} - \tilde{\omega}/\tilde{k})^2/4\tilde{T}}), \tag{3.87}$$

where we have used the first term of series expansion

$$\ln(1+x) = x - \frac{x^2}{2} + \ldots, \tag{3.88}$$

where $x = \pm z e^{-(\tilde{k}\pm\tilde{\omega}/\tilde{k})^2/4\tilde{T}}$. We have also assumed the $z \to 0$ limit at high temperatures. Let us simplify the result in Eq. (3.87)

$$\begin{aligned} S(\boldsymbol{k},\omega) &= \pm\frac{m\tilde{T}}{2\epsilon_0\tilde{k}}\frac{2\pi}{1-e^{-\tilde{\omega}/\tilde{T}}}e^{-(\tilde{k}^2+\tilde{\omega}^2/\tilde{k}^2)/4\tilde{T}}(\pm z e^{+\tilde{\omega}/2\tilde{T}} \mp z e^{-\tilde{\omega}/2\tilde{T}}) && (3.89)\\ &= \frac{m\tilde{T}}{2\epsilon_0\tilde{k}}\frac{2\pi}{e^{-\tilde{\omega}/2\tilde{T}}\sinh(\tilde{\omega}/2\tilde{T})}e^{-(\tilde{k}^2+\tilde{\omega}^2/\tilde{k}^2)/4\tilde{T}} z\sinh(\tilde{\omega}/2\tilde{T}) && (3.90)\\ &= \frac{2\pi m\tilde{T}}{2\epsilon_0\tilde{k}} z e^{-(\tilde{k}-\tilde{\omega}/\tilde{k})^2/4\tilde{T}}. && (3.91) \end{aligned}$$

The second term of the expansion in Eq. (3.88) yields the correction

$$S'(\boldsymbol{k},\omega) = S(\boldsymbol{k},\omega) + \frac{2\pi m\tilde{T}}{4\epsilon_0\tilde{k}} z^2 e^{-2(\tilde{k}-\tilde{\omega}/\tilde{k})^2/4\tilde{T}}\frac{\sinh(\tilde{\omega}/\tilde{T})}{\sinh(\tilde{\omega}/2\tilde{T})}. \tag{3.92}$$

By comparing Eqs. (3.92) and (3.58), one finds that in the high-temperature limit the structure factor of the quantum gas reduces to that for Maxwell-Boltzmann particles, Eq. (3.58).

3.4.3 Degenerate Bose gas

Let us calculate the $S(\boldsymbol{k},\omega)$ for a Bose gas in the low-temperature limit with $z \to 1$

$$\begin{aligned} S(\boldsymbol{k},\omega) &= \lim_{T\to 0}\frac{m\tilde{T}}{2\epsilon_0\tilde{k}}\frac{2\pi}{1-e^{-\tilde{\omega}/\tilde{T}}}\ln\left[\frac{1-ze^{-(\tilde{k}+\tilde{\omega}/\tilde{k})^2/4\tilde{T}}}{1-ze^{-(\tilde{k}-\tilde{\omega}/\tilde{k})^2/4\tilde{T}}}\right], && (3.93)\\ & && (3.94) \end{aligned}$$

where $\tilde{k} = k/k_0$, $\tilde{\omega} = \omega/\epsilon_0$, and $\tilde{T} = 1/\beta\epsilon_0$, where $k_0 = \rho^{1/3}$, $\epsilon_0 = k_0^2/2m$, and $z = e^{\mu/k_B T}$. In the limit $\tilde{T} \to 0$

$$z e^{-(\tilde{k}-\tilde{\omega}/\tilde{k})^2/4\tilde{T}} \to \begin{cases} 0 & \tilde{k} \neq \pm\tilde{\omega}/\tilde{k} \\ 1 & \tilde{k} = \tilde{\omega}/\tilde{k} \end{cases}. \tag{3.95}$$

Thus we obtain

$$S(\boldsymbol{k},\omega) = \frac{\tilde{T}}{\tilde{k}}\ln\left[1-ze^{(\tilde{\omega}/\tilde{k}-\tilde{k})^2/4\tilde{T}}\right] + n_0\left[\delta\left(\tilde{k}-\tilde{\omega}/\tilde{k}\right) - \delta\left(\tilde{k}+\tilde{\omega}/\tilde{k}\right)\right], \tag{3.96}$$

which is the structure factor for a degenerate Bose gas.

3.4.4 Degenerate Fermi gas

The distribution function of a degenerate Fermi gas in the momentum space is a step function

$$n_{\boldsymbol{p}} = \theta(p_{\mathrm{F}} - p), \tag{3.97}$$

where p_{F} is the Fermi momentum.

Substituting Eq. (3.97) into Eq. (3.38), we obtain

$$S(\boldsymbol{k},\omega) = \sum_{\boldsymbol{p},\boldsymbol{p}'} \theta(p_{\mathrm{F}} - p)\theta(p' - p_{\mathrm{F}})\, \delta(\boldsymbol{p} + \boldsymbol{k} - \boldsymbol{p}')\, \delta(\omega_{\boldsymbol{p}} + \omega - \omega_{\boldsymbol{p}'}). \tag{3.98}$$

Converting the sum into integrals and substituting $\boldsymbol{p}' = \boldsymbol{p} + \boldsymbol{k}$, we obtain

$$S(\boldsymbol{k},\omega) = \int d^3\boldsymbol{p}\theta(p_{\mathrm{F}} - p)\theta(p + k - p_{\mathrm{F}})\, \delta(\omega - \frac{p_z k}{m} - \frac{k^2}{2m}). \tag{3.99}$$

Introducing cylindrical coordinates and using the result in Eq. (3.49), we may write

$$S(\boldsymbol{k},\omega) = -\frac{2\pi m}{k} \int_{-k/2}^{p_{\mathrm{F}}} dp_z \int_{p_{\perp\min}(p_z)}^{p_{\perp\max}(p_z)} p_\perp dp_\perp \delta\left(p_z - \frac{m\omega}{k} + \frac{k}{2}\right). \tag{3.100}$$

This integral has a geometrical interpretation, illustrated in Fig. 3.6. The integration area may be divided into two areas discussed separately.

Consider first the area 1 in Fig. 3.6, where $p_{\mathrm{F}} - k \leq p_z \leq p_{\mathrm{F}}$. Equally, we may require $\frac{p_{\mathrm{F}}k}{m} - \frac{k^2}{2m} \leq \omega \leq \frac{p_{\mathrm{F}}k}{m} + \frac{k^2}{2m}$. Then Eq. (3.100) assumes the form

$$\begin{aligned}
S(\boldsymbol{k},\omega) &= -\frac{2\pi m}{k} \int_{p_{\mathrm{F}}-k}^{p_{\mathrm{F}}} dp_z \int_0^{\sqrt{p_{\mathrm{F}}^2 - p_z^2}} p_\perp dp_\perp \delta(p_z - \frac{m\omega}{k} + \frac{k}{2}) && (3.101)\\
&= -\frac{2\pi m}{k} \int_{p_{\mathrm{F}}-k}^{p_{\mathrm{F}}} dp_z \frac{1}{2} \left(\sqrt{p_{\mathrm{F}}^2 - p_z^2}\right)^2 \delta(p_z - \frac{m\omega}{k} + \frac{k}{2}) && (3.102)\\
&= -\frac{2\pi m}{k}\frac{1}{2}\left(p_{\mathrm{F}}^2 - \left(\frac{m\omega}{k} - \frac{k}{2}\right)^2\right) && (3.103)\\
&= -\frac{\pi m}{k}\left(p_{\mathrm{F}}^2 - \left(\frac{m\omega}{k} - \frac{k}{2}\right)^2\right). && (3.104)
\end{aligned}$$

Consider the case in which $-\frac{k}{2} < p_z < p_{\mathrm{F}} - k \Leftrightarrow 0 < \omega < \frac{p_{\mathrm{F}}k}{m} - \frac{k^2}{2m}$, area 2 in Fig. 3.6. Here we have

$$S(\boldsymbol{k},\omega) = -\frac{2\pi m}{k} \int_{-k/2}^{p_{\mathrm{F}}-k} dp_z \int_{\sqrt{p_{\mathrm{F}}^2 - (p_z + k/2)^2}}^{\sqrt{p_{\mathrm{F}}^2 - p_z^2}} p_\perp dp_\perp \delta\left(p_z - \frac{m\omega}{k} + \frac{k}{2}\right) \tag{3.105}$$

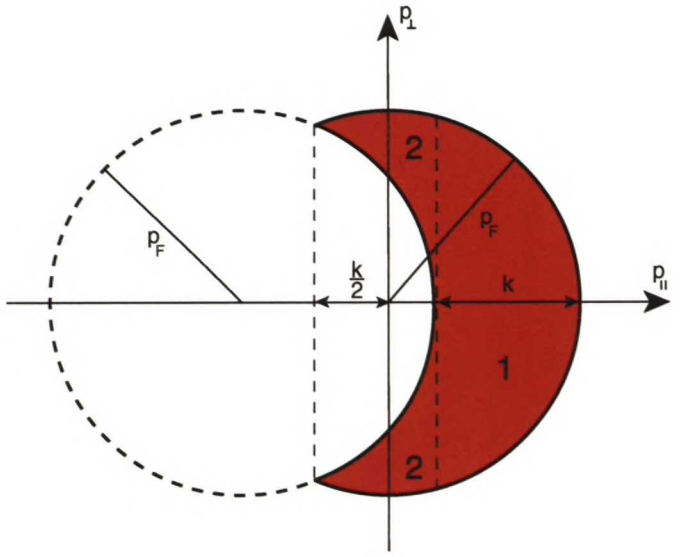

Figure 3.6: Red crescent represents the excitations induced in a degenerate Fermi system when probed with particles of momentum $\boldsymbol{k}$.

$$
\begin{aligned}
&= -\frac{2\pi m}{k}\int_{-k/2}^{p_F-k} dp_z \delta\left(p_z - \frac{m\omega}{k} + \frac{k}{2}\right) \\
&\quad \times \frac{1}{2}\left[\left(\sqrt{p_F^2 - p_z^2}\right)^2 - \left(\sqrt{p_F^2 - p_z^2 - 2p_z k - k^2}\right)^2\right] && (3.106)\\
&= -\frac{\pi m}{k}\left[p_F^2 - p_z^2 - p_F^2 + p_z^2 + 2p_z k + k^2\right] && (3.107)\\
&= -\frac{\pi m}{k}\left(2(\frac{m\omega}{k} - \frac{k}{2})k + k^2\right) && (3.108)\\
&= -\frac{2\pi m^2 \omega}{k}. && (3.109)
\end{aligned}
$$

By dividing the results in (3.104) and (3.109) with the volume of the Fermi sphere, $\frac{4}{3}\pi p_F^3$, and multiplying by the total number of particles in the systen N, we obtain

$$
S(\boldsymbol{k},\omega) = \begin{cases} \frac{3m^2 N\omega}{2kp_F^3} & 0 \le \omega \le \frac{p_F k}{m} - \frac{k^2}{2m} \\ \frac{3mN}{4kp_F}\left(1 - \left[\frac{m\omega}{kp_F} - \frac{k}{2p_F}\right]^2\right) & \frac{p_F k}{m} - \frac{k^2}{2m} \le \omega \le \frac{p_F k}{m} + \frac{k^2}{2m} \\ 0 & \frac{p_F k}{m} + \frac{k^2}{2m} \le \omega. \end{cases} \qquad (3.110)
$$

The same result may be obtained from Eq. (3.68) in the low-temperature limit.

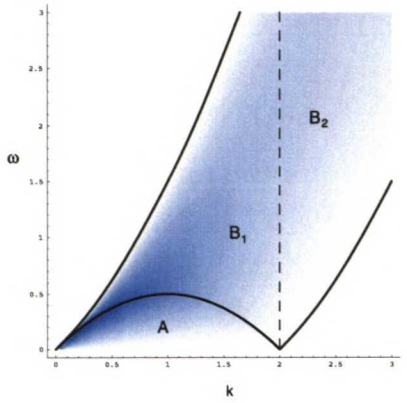

Figure 3.7: Structure factor for a degenerate noninteracting Fermi gas. The blue color means high values, boundaries of the integration areas are marked with lines.

3.4.5 Bose-Einstein and Fermi condensates

In the low-temperature limit, the quantum gases are fully degenerate; all the atoms are in the lowest possible energy state. First we consider a BEC, where all the atoms occupy the same ground state. Thus Eq. (3.96) reduces to

$$S(\boldsymbol{k},\omega) = n_0\left[\delta\left(\tilde{k}-\tilde{\omega}/\tilde{k}\right) - \delta\left(\tilde{k}+\tilde{\omega}/\tilde{k}\right)\right], \tag{3.111}$$

where n_0 is the number of particles in the BEC.

In a fully degenerate Fermi gas, the atoms occupy the lowest energy states up to the Fermi energy. When an attractive interaction is introduced between the atoms, the BCS-pairing of atoms is formed. The energy difference between the free and the paired state of the atoms is denoted by $\Delta/2$. Thus, due to the pairing, there exists a finite energy gap Δ in the excitation spectrum, $-\omega = \omega_{\boldsymbol{p}} + \omega_{\boldsymbol{p}-\boldsymbol{k}} > |\Delta|$. In Ref. [46], the dynamic structure function for incoherent scattering with $\boldsymbol{k} \neq 0$ is written as

$$S(\boldsymbol{k},\omega) = \frac{1}{4}\sum_{\boldsymbol{p}} \delta(\omega_{\boldsymbol{p}}+\omega+\omega_{\boldsymbol{k}-\boldsymbol{p}}) \left[\frac{\delta}{\omega_{\boldsymbol{p}}\omega_{\boldsymbol{k}-\boldsymbol{p}}} + \left(1-\frac{\xi_{\boldsymbol{p}}}{\omega_{\boldsymbol{p}}}\right)\left(1+\frac{\xi_{\boldsymbol{p}-\boldsymbol{k}}}{\omega_{\boldsymbol{p}-\boldsymbol{k}}}\right)\right], \tag{3.112}$$

where $E_{\boldsymbol{k}} = \sqrt{\Delta^2+\xi_{\boldsymbol{k}}^2}$, the quasiparticle energy with respect to the Fermi surface is $\xi_{\boldsymbol{k}} = \epsilon_k - \mu + \hbar u_g(\rho_\uparrow + \rho_\downarrow)/2$, and the strength of the contact interaction is $u_g = 4\pi a\hbar/m$. The explicit structure of the quasiparticle spectrum depends on the properties of the atoms.

4 Momentum transfer calculations

4.1 Interpenetrating systems

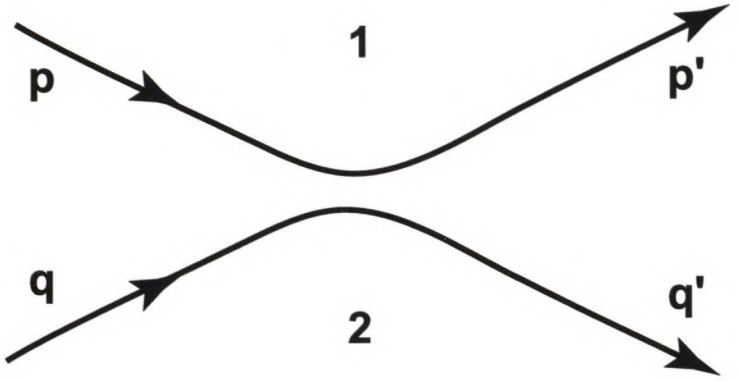

Figure 4.1: Schematic of the momentum transfer between two systems.

Let us consider two quantum systems passing through each other, see Fig. 4.1. System 1 transfers the momentum $\boldsymbol{k} = \boldsymbol{p}' - \boldsymbol{p}$ to system 2. The measurement of the momentum transfer yields a result which is the statistical average of the transitions through all the allowed interaction channels. For systems with a number of internal degrees of freedom and strong interactions, several interaction channels yield a significant contribution. One can handle the increasing variety of possible interaction channels by considering the Feynman diagrams, such as those in Fig. 4.2. The diagrams may be separated into groups through the order of the interaction. The group of first-order interactions consists of only one diagram, but their number increases very rapidly in the higher orders. Fortunately, for a weakly interacting dilute atomic gas it is a fair approximation to consider only the interactions in the first order. We omit the complicated calculations arising from the Feynman diagrams and set the effective matrix element $M_{\boldsymbol{p}} = 1$.

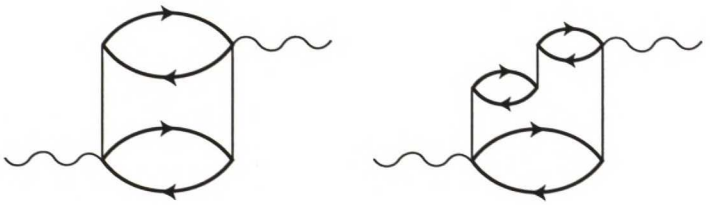

Figure 4.2: Feynman diagrams of the particle-particle scattering and one of the second-order scattering channels.

4.2 Momentum transfer rate

Here we consider the momentum transfer between two quantum systems. We derive the expression for the momentum transfer rate, and show that when studied only to the first order in $\boldsymbol{v}$, it simplifies into the form

$$\frac{\mathrm{d}\boldsymbol{P}_1}{\mathrm{dt}} = -\frac{\boldsymbol{v}}{6}\int \frac{d^3k}{(2\pi)^3}\, k^2\, |M_{\boldsymbol{k}}|^2 \left[\beta \int_{-\infty}^{\infty} \frac{d\omega}{2\pi}\, S_1(\boldsymbol{k},\omega)\, S_2(\boldsymbol{k},-\omega)\right], \tag{4.1}$$

where we have defined the dynamic structure factors

$$S_1(\boldsymbol{k},\omega) = \sum_{\boldsymbol{p}\,\boldsymbol{p}'} n_{\boldsymbol{p}}(1 \pm n_{\boldsymbol{p}'})\, \delta(\boldsymbol{p}+\boldsymbol{k}-\boldsymbol{p}')\, \delta(\omega_{\boldsymbol{p}}+\omega-\omega_{\boldsymbol{p}'}) \tag{4.2}$$

$$S_2(\boldsymbol{k},\omega) = \sum_{\boldsymbol{q}\,\boldsymbol{q}'} f^0_{\boldsymbol{q}}(1 \pm f^0_{\boldsymbol{q}'})\, \delta(\boldsymbol{q}+\boldsymbol{k}-\boldsymbol{q}')\, \delta(\omega_{\boldsymbol{q}}+\omega-\omega_{\boldsymbol{q}'}). \tag{4.3}$$

Let us rewrite the distribution function for a quantum gas

$$n_{\boldsymbol{p}} = \frac{1}{e^{\beta(\epsilon-\mu)} \pm 1}, \tag{4.4}$$

where the upper sign stands for fermions and the lower one for bosons. By direct calculation one finds

$$\frac{\partial n_{\boldsymbol{p}}}{\partial \epsilon} = \frac{-\beta\, e^{\beta(\epsilon-\mu)}}{(e^{\beta(\epsilon-\mu)} \pm 1)^2} = -\beta\, n_{\boldsymbol{p}}(1 \mp n_{\boldsymbol{p}}). \tag{4.5}$$

Let us linearize $n_{\boldsymbol{p}}$ by including the first two terms in its Taylor series

$$n_{\boldsymbol{p}} = n^0_{\boldsymbol{p}} - \frac{\partial\, n^0_{\boldsymbol{p}}}{\partial \boldsymbol{v}} \cdot \boldsymbol{v} + \ldots \tag{4.6}$$

$$= n^0_{\boldsymbol{p}} - \frac{\partial\, n^0_{\boldsymbol{p}}}{\partial \epsilon}\frac{\partial\, \epsilon}{\partial \boldsymbol{v}} \cdot \boldsymbol{v} + \ldots \tag{4.7}$$

$$\approx n^0_{\boldsymbol{p}} + \beta\, n^0_{\boldsymbol{p}}(1 \mp n^0_{\boldsymbol{p}})\, \boldsymbol{p} \cdot \boldsymbol{v}. \tag{4.8}$$

The first term omitted in the series is

$$\frac{1}{2}\frac{\partial^2 n_{\boldsymbol{p}}^0}{\partial \boldsymbol{v}^2}\boldsymbol{v}^2 = \frac{1}{2}\beta^2 n_{\boldsymbol{p}}^0(1\mp n_{\boldsymbol{p}}^0)(1\mp 2n_{\boldsymbol{p}}^0)\boldsymbol{p}^2\boldsymbol{v}^2. \tag{4.9}$$

Using the series expansion, we may write to the linear order in $\boldsymbol{v}$

$$n_{\boldsymbol{p}}^0(1\mp n_{\boldsymbol{p}'}^0) = n_{\boldsymbol{p}}^0(1\mp n_{\boldsymbol{p}'}^0) + \beta n_{\boldsymbol{p}}^0(1\mp n_{\boldsymbol{p}'}^0)\left[(1\mp n_{\boldsymbol{p}}^0)\,\boldsymbol{p}\cdot\boldsymbol{v} - n_{\boldsymbol{p}'}^0\,\boldsymbol{p}'\cdot\boldsymbol{v}\right]. \tag{4.10}$$

Let us rewrite Eq. (3.20) using expressions (4.10) and (4.3)

$$\begin{aligned}\frac{\mathrm{d}\boldsymbol{P}_1}{\mathrm{dt}} &= \sum_{\boldsymbol{p}\boldsymbol{p}'}(\boldsymbol{p}-\boldsymbol{p}')|M|^2 S_2(\boldsymbol{p}-\boldsymbol{p}',\omega_{\boldsymbol{p}}-\omega_{\boldsymbol{p}'})\,n_{\boldsymbol{p}}^0(1\mp n_{\boldsymbol{p}'}^0)\\ &\quad\times\left(1+\beta\left[(1\mp n_{\boldsymbol{p}}^0)\,\boldsymbol{p}\cdot\boldsymbol{v} - n_{\boldsymbol{p}'}^0\,\boldsymbol{p}'\cdot\boldsymbol{v}\right]\right).\end{aligned} \tag{4.11}$$

Observe that $S_2(\boldsymbol{p}-\boldsymbol{p}',\omega_{\boldsymbol{p}}-\omega_{\boldsymbol{p}'})n_{\boldsymbol{p}}^0(1\pm n_{\boldsymbol{p}'}^0)$ is symmetric under the interchange $\boldsymbol{p}\leftrightarrow\boldsymbol{p}'$. It follows that

$$\sum_{\boldsymbol{p}\boldsymbol{p}'}(\boldsymbol{p}-\boldsymbol{p}')|M|^2 S_2(\boldsymbol{p}-\boldsymbol{p}',\omega_{\boldsymbol{p}}-\omega_{\boldsymbol{p}'})n_{\boldsymbol{p}}^0(1\mp n_{\boldsymbol{p}'}^0) = 0. \tag{4.12}$$

Thus Eq. (4.11) reduces to

$$\begin{aligned}\frac{\mathrm{d}\boldsymbol{P}_1}{\mathrm{dt}} &= \beta\sum_{\boldsymbol{p}\boldsymbol{p}'}(\boldsymbol{p}-\boldsymbol{p}')|M|^2 S_2(\boldsymbol{p}-\boldsymbol{p}',\omega_{\boldsymbol{p}}-\omega_{\boldsymbol{p}'})n_{\boldsymbol{p}}^0(1\mp n_{\boldsymbol{p}'}^0)\\ &\quad\times\left[(1\mp n_{\boldsymbol{p}}^0)\,\boldsymbol{p}\cdot\boldsymbol{v}\mp n_{\boldsymbol{p}'}^0\,\boldsymbol{p}'\cdot\boldsymbol{v}\right].\end{aligned} \tag{4.13}$$

Using the same symmetry argument as above, we may write

$$\begin{aligned}(1\mp n_{\boldsymbol{p}}^0)\,\boldsymbol{p}\cdot\boldsymbol{v}\mp n_{\boldsymbol{p}'}^0\,\boldsymbol{p}'\cdot\boldsymbol{v} &= \frac{1}{2}\left[(1\mp n_{\boldsymbol{p}}^0)\,\boldsymbol{p}\cdot\boldsymbol{v}\,pn_{\boldsymbol{p}'}^0\,\boldsymbol{p}'\cdot\boldsymbol{v}\right.\\ &\quad\left.-(1\mp n_{\boldsymbol{p}'}^0)\,\boldsymbol{p}'\cdot\boldsymbol{v}\pm n_{\boldsymbol{p}}^0\,\boldsymbol{p}\cdot\boldsymbol{v})\right] &(4.14)\\ &= \frac{1}{2}(\boldsymbol{p}-\boldsymbol{p}')\cdot\boldsymbol{v}. &(4.15)\end{aligned}$$

Substituting Eq. (4.15) into (4.13) we obtain

$$\begin{aligned}\frac{\mathrm{d}\boldsymbol{P}_1}{\mathrm{dt}} &= \frac{\beta}{2}\sum_{\boldsymbol{p}\boldsymbol{p}'}(\boldsymbol{p}-\boldsymbol{p}')|M|^2\,(\boldsymbol{p}-\boldsymbol{p}')\cdot\boldsymbol{v}\\ &\quad\times S_2(\boldsymbol{p}-\boldsymbol{p}',\omega_{\boldsymbol{p}}-\omega_{\boldsymbol{p}'})n_{\boldsymbol{p}}^0(1\mp n_{\boldsymbol{p}'}^0).\end{aligned} \tag{4.16}$$

By introducing the new variables $\boldsymbol{k} = \boldsymbol{p} - \boldsymbol{p}'$ and $\boldsymbol{q} = \boldsymbol{p}'$, we obtain

$$\frac{\mathrm{d}\boldsymbol{P}_1}{\mathrm{dt}} = \boldsymbol{v}\frac{\beta}{2}\sum_{\boldsymbol{k}}\sum_{\boldsymbol{q}}|M|^2k^2S_2(k,\omega_{\boldsymbol{k}+\boldsymbol{q}}-\omega_{\boldsymbol{q}})n^0_{\boldsymbol{k}+\boldsymbol{q}}(1\mp n^0_{\boldsymbol{q}}). \tag{4.17}$$

As we see from Eq. (4.3), S_2 consists of Kronecker's delta functions $\delta(\boldsymbol{q}+\boldsymbol{k}-\boldsymbol{q}')$ and $\delta(\omega_{\boldsymbol{q}}+\omega-\omega_{\boldsymbol{q}'})$. The expression is invariant if we introduce Kronecker's delta once more

$$\begin{aligned}\frac{\mathrm{d}\boldsymbol{P}_1}{\mathrm{dt}} = \boldsymbol{v}\frac{\beta}{2}\sum_{\boldsymbol{k}}|M|^2k^2\sum_{\boldsymbol{q}}S_2(k,\omega_{\boldsymbol{k}+\boldsymbol{q}}-\omega_{\boldsymbol{q}}) \\ \times n^0_{\boldsymbol{k}+\boldsymbol{q}}(1\pm n^0_{\boldsymbol{q}})\delta(\boldsymbol{q}+\boldsymbol{k}-\boldsymbol{q}')\delta(\omega_{\boldsymbol{q}}+\omega-\omega_{\boldsymbol{q}'}).\end{aligned} \tag{4.18}$$

Here we can recognize the structure of $S_1(\boldsymbol{k},\omega)$

$$S_1(\boldsymbol{k},\omega) = \sum_{\boldsymbol{p}\,\boldsymbol{p}'} n_{\boldsymbol{p}}(1\mp n_{\boldsymbol{p}'})(2\pi)^4\,\delta(\boldsymbol{p}+\boldsymbol{k}-\boldsymbol{p}')\,\delta(\omega_{\boldsymbol{p}}+\omega-\omega_{\boldsymbol{p}'}). \tag{4.19}$$

Thus Eq. (4.17) may be written in the form of a convolution of dynamic structure factors for the two systems

$$\frac{\mathrm{d}\boldsymbol{P}_1}{\mathrm{dt}} = \boldsymbol{v}\frac{\beta}{2}\sum_{\boldsymbol{k}}|M|^2k^2\sum_{\boldsymbol{q}}S_1(k,\omega_{\boldsymbol{k}+\boldsymbol{q}}-\omega_{\boldsymbol{q}})S_2(k,\omega_{\boldsymbol{q}}-\omega_{\boldsymbol{q}+\boldsymbol{k}}). \tag{4.20}$$

By converting the sum over $\boldsymbol{q}$ into an integration over ω we finally obtain [1]

$$\frac{\mathrm{d}\boldsymbol{P}_1}{\mathrm{dt}} = -\frac{\boldsymbol{v}}{6}\int\frac{d^3k}{(2\pi)^3}\,k^2\,|M_{\boldsymbol{k}}|^2\left[\beta\int_{-\infty}^{\infty}\frac{d\omega}{2\pi}\,S_1(\boldsymbol{k},\omega)\,S_2(\boldsymbol{k},-\omega)\right], \tag{4.21}$$

which describes the rate of momentum transfer from system 1 to system 2.

4.3 Impurity motion

Here we consider the motion of fast and heavy impurities immersed to an ideal gas. We have the relation in Eq. (3.27) between the mobility and the momentum transfer rate

$$\frac{\langle\boldsymbol{v}\rangle}{\mu} = \frac{d\boldsymbol{P}}{dt} = -\frac{\boldsymbol{v}\beta}{6}\int\frac{dk}{(2\pi)^3}\,k^4\int_{-\infty}^{\infty}d\omega\;S(\boldsymbol{k},\omega)\,N_2\delta\left(-\omega-\frac{k^2}{2m_2}\right), \tag{4.22}$$

Below we study the mobility of the impurity applying different structure factors $S(\boldsymbol{k},\omega)$ in Eq. (4.22).

[1] Now the delta functions in ω change from discrete Kronecker delta's to Dirac's delta functions. However, we must keep in mind the discrete backround of the theory and, therefore, we can "simplify" the undefined expressions, such as $\delta(x)\,\delta(-x) = \delta(x)$.

i) Impurity in a classical gas

We find an analytic expression for the momentum transfer rate

$$\begin{aligned}\frac{d\boldsymbol{P}}{dt} &= -\frac{\boldsymbol{v}\beta}{6}\int\frac{dk}{(2\pi)^3}k^4\int_{-\infty}^{\infty}d\omega\,\frac{\sqrt{2\pi m_1\beta}}{k}N_1N_2 \\ &\quad\times e^{\frac{-\beta m_1}{2k^2}(\omega-\frac{k}{2m_1})^2}\delta\left(-\omega-\frac{k^2}{2m_2}\right) \qquad (4.23)\\ &= -\frac{\boldsymbol{v}\beta\sqrt{2\pi m_1\beta}N_1N_2}{6}\int\frac{dk}{(2\pi)^3}k^3e^{\frac{-\beta m_1k^2}{4}(\frac{1}{m_1}+\frac{1}{m_2})^2} \qquad (4.24)\\ &= -\frac{\boldsymbol{v}\beta\sqrt{2\pi m_1\beta}N_1N_2}{6}\frac{8m_1^6m_2^8}{m_1^2+m_2^2)^4\beta^2} \qquad (4.25)\\ &= -\frac{\boldsymbol{v}\sqrt{2\pi m_1}N_1N_2}{6}\frac{8m_1^6m_2^8}{(m_1^2+m_2^2)^4}(k_{\mathrm{B}}T)^{1/2}. \qquad (4.26)\end{aligned}$$

The result above is important since deviations from it reveal quantum-statistical effects.

ii) Impurity in a quantum gas.

Let us reformulate the expression for momentum transfer rate

$$\begin{aligned}\frac{d\boldsymbol{P}}{dt} &= -\frac{\boldsymbol{v}\beta}{6}\int\frac{m\tilde{T}}{2\epsilon_0\tilde{k}}\frac{2\pi}{1-e^{-\tilde{\omega}/\tilde{T}}} \\ &\quad\times\ln\left[\frac{1\mp ze^{-(k^2+2m_1\omega)^2/8mk^2T}}{1\mp ze^{-(k^2-2m_1\omega)^2/8mk^2T}}\right]\delta\left(-\tilde{\omega}-\frac{\tilde{k}^2}{2m}\right). \qquad (4.27)\end{aligned}$$

The fugacity z is related to the number of particles N_1

$$N=\int d\boldsymbol{p}\,\frac{1}{ze^{p^2/(2mk_{\mathrm{B}}T)}\mp 1}, \qquad (4.28)$$

where $(\mp)$ stands for bosons (fermions). For bosons or fermions, the fugacity has no analytic form in terms of N. In the classical limit $T\to\infty$, we find the limiting behavior for $z\approx T^{-3/2}$ for both bosons and fermions. In the low-temperature limit, the difference in z is crucial. In a Fermi gas, when $T\to 0$, the Fermi-Dirac distribution becomes a step function. We find for the fugacity $z\approx e^{\epsilon_{\mathrm{F}}/k_{\mathrm{B}}T}$, where ϵ_{F} is the Fermi energy. In a Bose gas, the fugacity $z\to 1$ as $T\to T_{\mathrm{BEC}}$. Below T_{BEC}, the integration over the Bose-Einstein distribution function gives a particle number smaller than N; thus $z=1$.

We calculated the fugacity z numerically for some temperatures T and then substituted the resolved values to equation of momentum transfer rate. Finally, we obtained the temperature dependence of the mobility evaluating expression in Eq. (4.27) using numerical integration. The results are shown in Figs. 4.3.

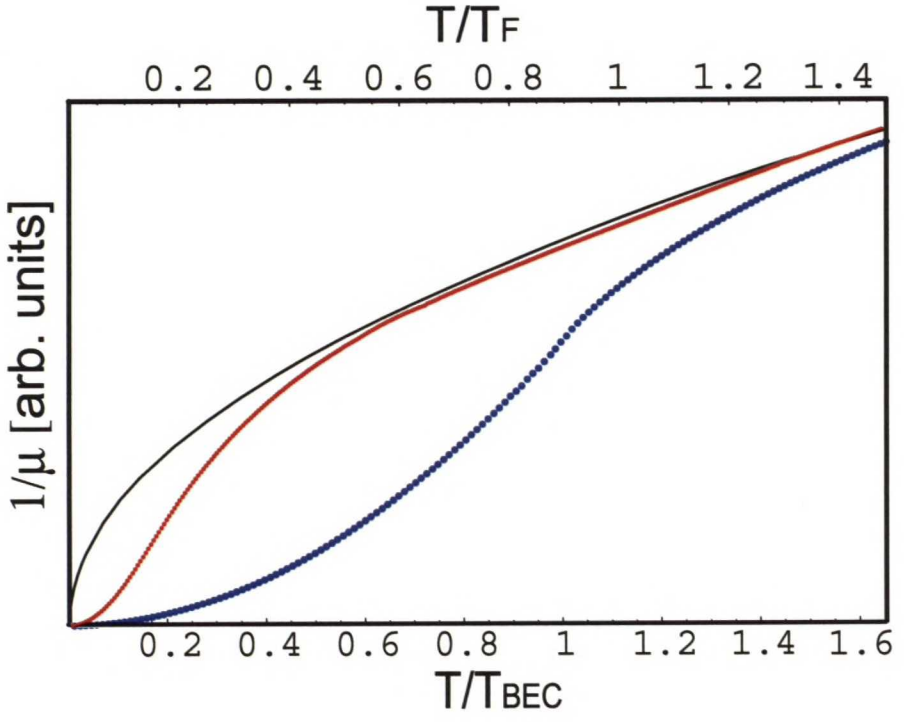

Figure 4.3: Mobility of the impurity. The points are the numerical results obtained for the impurity moving in a Fermi (red points) and a Bose (blue points) gas. The black line is the result for a classical gas. The mass of the impurity was ten times the mass of the gas atoms.

4.4 Momentum transfer between gases

Here we consider various combinations of interpenetrating Maxwell-Boltzmann, Fermi and Bose gases. The calculation of $d\boldsymbol{P}/dt$ is accomplished as above. First, the fugacity z is evaluated from Eq. (4.28). The fugacity is substituted into Eq. (4.1), and the rate of momentum transfer $d\boldsymbol{P}/dt$ is obtained. The calculation is carried out analytically only for the case of two Maxwell-Boltzmann gases. Otherwise, we use numerical methods.

4.4.1 Gas in a Maxwell-Boltzmann gas

Consider the rate of momentum transfer between two interpenetrating classical gases moving with respect to each other with the velocity $\boldsymbol{v}$. Let the gas 1 consists of N_1 particles with mass m_1 and gas 2 of N_2 particles mass m_2. Let us denote the temperature of the gases by $T = 1/k_B\beta$. There is no angular dependence in $S(\boldsymbol{k}, \omega)$ so we may write

$$\frac{d\boldsymbol{P}}{dt} = -\frac{\boldsymbol{v}\beta}{6} \int \frac{dk}{(2\pi)^3} k^4 \int_{-\infty}^{\infty} d\omega \; S_1(\boldsymbol{k}, \omega) \, S_2(\boldsymbol{k}, -\omega), \tag{4.29}$$

where

$$S_1(\boldsymbol{k}, \omega) = \frac{\sqrt{2\pi m_1 \beta}}{k} N_1 e^{\frac{-\beta m_1}{2k^2}(\omega - \frac{k}{2m_1})^2} \tag{4.30}$$

$$S_2(\boldsymbol{k}, -\omega) = \frac{\sqrt{2\pi m_2 \beta}}{k} N_2 e^{\frac{-\beta m_2}{2k^2}(-\omega - \frac{k}{2m_2})^2}. \tag{4.31}$$

The calculation of the integral over ω yields

$$\int_{-\infty}^{\infty} S(\boldsymbol{k}, \omega) S(\boldsymbol{k}, -\omega) d\omega = \frac{(2\pi)^{3/2}}{k} N_1 N_2 \sqrt{\beta \frac{m_1 m_2}{m_1 + m_2}} e^{-\beta \frac{k^2}{8} \frac{(m_1 + m_2)}{m_1 m_2}}. \tag{4.32}$$

By integrating over k, one obtains

$$\frac{d\boldsymbol{P}}{dt} = -\frac{\boldsymbol{v}\beta}{6} \int \frac{dk}{(2\pi)^3} k^4 \frac{(2\pi)^{3/2}}{k} N_1 N_2 \sqrt{\beta \frac{m_1 m_2}{m_1 + m_2}} e^{-\beta \frac{k^2}{8} \frac{(m_1 + m_2)}{m_1 m_2}} \tag{4.33}$$

$$= -\frac{\boldsymbol{v}\beta}{6} \frac{32 N_1 N_2}{(2\pi)^{3/2}} \left(\frac{m_1 m_2}{m_1 + m_2} \right)^{5/2} \beta^{-1/2} \tag{4.34}$$

$$= -\frac{16\boldsymbol{v}}{3} \frac{N_1 N_2}{(2\pi)^{1/2}} \left(\frac{m_1 m_2}{m_1 + m_2} \right)^{5/2} (k_B T)^{1/2}. \tag{4.35}$$

The temperature dependence $T^{1/2}$ of the Eq. (4.35) is the asymptotical behavior for all gases in the limit $T \to \infty$. Below, we have plotted $d\boldsymbol{P}/dt$ as a function of temperature T, see Fig. 4.4. In the low-temperature limit, we find the rate of the momentum transfer vanishing as T^2 for both the Fermi-Maxwell-Boltzmann and Bose-Maxwell-Boltzmann cases.

4.4.2 Two quantum gases

Finally we consider the system of two quantum gases. The temperature dependence of $d\boldsymbol{P}/dt$ is shown in Fig. 4.5 for all the possible combinations of quantum

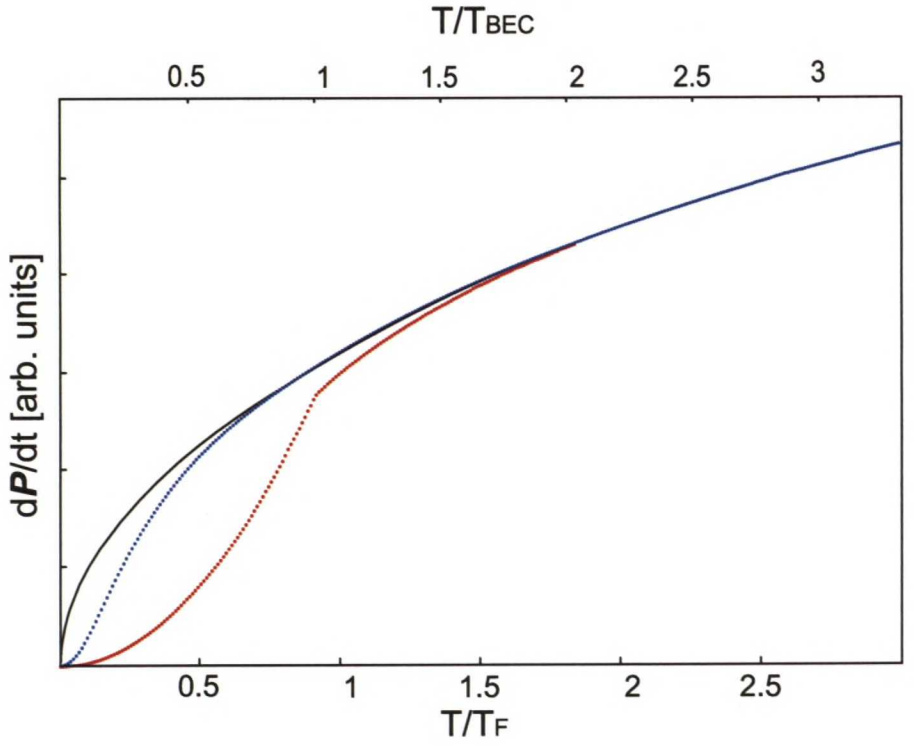

Figure 4.4: Mobility in the classical gas. The red points represent the momentum transfer for a Bose gas and the blue points for a Fermi gas. The black line is the result for a classical gas.

gases. In the low-temperature limit, the momentum transfer rate vanished as T^2 for the Fermi-Fermi, $T^{7/2}$ for the Bose-Bose, and T^3 for the Bose-Fermi cases.

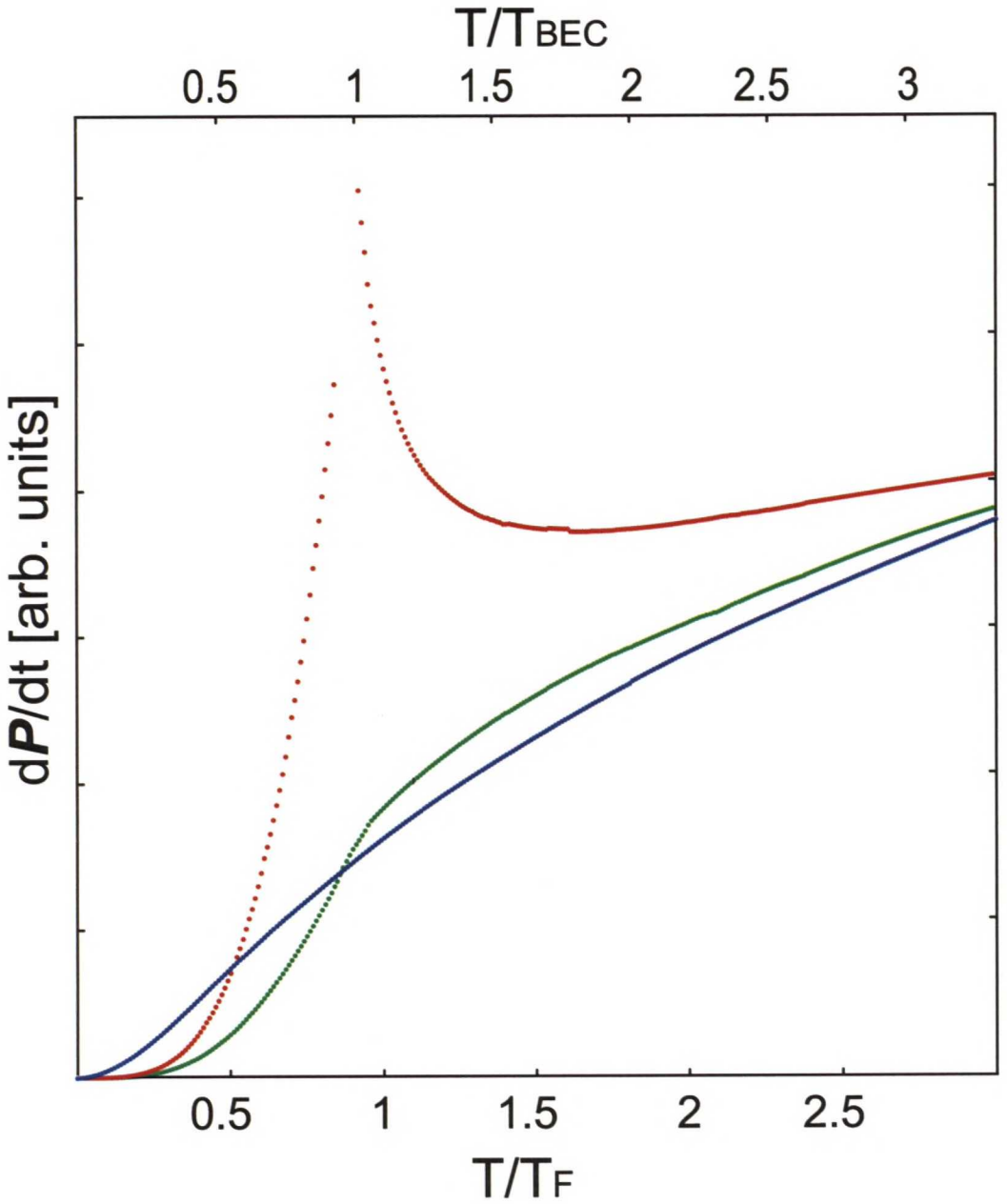

Figure 4.5: Momentum transfer rate between interpenetrating quantum gases. The point symbols represent the rate of momentum transfer between Bose-Bose (red), Fermi-Fermi (blue), and Bose-Fermi (green) gases. The numerical results are computed for gases consisting of atoms with equal masses.

5 Discussion

The momentum transfer between atomic gases has been studied. The work consists of considerations of the low-temperature atomic gas experiments, study of linear response theory, and the calculation of the momentum transfer between ideal gases and the impurity motion.

The atomic gas experiments are establishing their place as an extremely sensitive test bench of quantum mechanics. The methods needed for cooling the gases down to the BEC transition temperatures are gradually becoming well known. The research is concentrating on the properties of degenerate gases and methods to manipulate them. The next major challenge is the observation of a BCS transition in Fermi gases. However, the atomic gases turn into superfluid near 0 K, which harmfully affects the attempts to cool them. Due this decoupling of interactions, future investigations will almost certainly require a many-component degenerate atom system. The latter part of this work answered to the question of how quickly does the momentum transfer between the atomic gases vanish as $T \to 0$.

The rich physics displayed by the cold dilute atomic gases is based essentially on s-wave scattering and linear response. We reviewed linear response theory, which provides the formalism to handle many-body quantum systems. The general discussion on the linear response functions link quantum-statistical expectation values to the experimental quantities. The analytic expressions for the dynamic structure factor $S(\boldsymbol{k}, \omega)$ was found for the ideal gases with different statistics. Finally, the expression for the momentum transfer rate, $d\boldsymbol{P}/dt$, between interpenetrating quantum systems was found.

The calculations of $S(\boldsymbol{k}, \omega)$ and those of $d\boldsymbol{P}/dt$ are in agreement with the experiments of Refs. [31, 21]. In the quantum gas, the momentum-transfer rate is suppressed. In the Fermi gas, due to the Pauli exclusion principle and, in the Bose gas, due to the formation of the Bose-Einstein condensate. The effect of the suppression was yield power-law behavior for $d\boldsymbol{P}/dt$ in the low-temperature

limit.

It may be concluded that quantum-statistical features dominate the properties of the atomic gases in the low-temperature limit. The results yield information on the behavior of quantum systems at low temperatures. The results may also give ideas for improving the cooling strategies for atomic gases and to understand the experimental result on impurity motion and the motion of interpenetrating quantum gases.

Table of structure factors

System	$S(\boldsymbol{k},\omega)$	Remarks
Ideal Maxwell-Bolztmann	$\frac{m^2}{2\pi\beta k}e^{\beta\mu}e^{-\frac{\beta m}{2k^2}(\omega-\frac{\beta k^2}{2m})^2}$	$\beta = 1/k_{\mathrm{B}}T$
Ideal Fermi	$\frac{m\tilde{T}}{2\epsilon_0\tilde{k}}\frac{2\pi}{1-e^{-\tilde{\omega}/\tilde{T}}}\ln\left[\frac{1+e^{-(\tilde{k}-\tilde{\omega}/\tilde{k})^2/4\tilde{T}+1/\tilde{T}}}{1+e^{-(\tilde{k}+\tilde{\omega}/\tilde{k})^2/4\tilde{T}+1/\tilde{T}}}\right]$	$\tilde{k} = k/k_{\mathrm{F}}$, $\tilde{\omega} = \omega/\epsilon_{\mathrm{F}}$, $\tilde{T} = 1/\beta\epsilon_{\mathrm{F}}$, and $\epsilon_{\mathrm{F}} = k_{\mathrm{F}}^2/2m$
Ideal Bose	$\frac{m\tilde{T}}{2\epsilon_0\tilde{k}}\frac{1}{1-e^{-\tilde{\omega}/\tilde{T}}}\ln\left[\frac{1-ze^{-(\tilde{k}+\tilde{\omega}/\tilde{k})^2/4\tilde{T}}}{1-ze^{-(\tilde{k}-\tilde{\omega}/\tilde{k})^2/4\tilde{T}}}\right]$ $+\frac{1}{1-e^{-\tilde{\omega}/\tilde{T}}}\left[\delta(\tilde{\omega}-\tilde{k^2})-\delta(\tilde{\omega}-\tilde{k^2})\right]$	$\tilde{k} = k/k_0$, $\tilde{\omega} = \omega/\epsilon_0$, $\tilde{T} = 1/\beta\epsilon_0$, $k_0 = \rho^{1/3}$, $\epsilon_0 = k_0^2/2m$, and $z = e^{\mu/k_{\mathrm{B}}T}$
Recoilless	$N\delta\left(\omega-\frac{k^2}{2m}\right)$	
Degenerate Bose	$\frac{\tilde{T}}{\tilde{k}}\ln\left[1-ze^{(\tilde{\omega}/\tilde{k}-\tilde{k})^2/4\tilde{T}}\right]$ $+n_0\left[\delta\left(\tilde{k}-\tilde{\omega}/\tilde{k}\right)-\delta\left(\tilde{k}+\tilde{\omega}/\tilde{k}\right)\right]$	$\tilde{k} = k/k_0$, $\tilde{\omega} = \omega/\epsilon_0$, $\tilde{T} = 1/\beta\epsilon_0$, $k_0 = \rho^{1/3}$, $\epsilon_0 = k_0^2/2m$, and $z = e^{\mu/k_{\mathrm{B}}T}$
Degenerate Fermi	$\frac{3m^2N\omega}{2kp_{\mathrm{F}}^3}\quad 0\le\omega\le\omega_1$ $\frac{3mN}{4kp_{\mathrm{F}}}\left(1-\left[\frac{m\omega}{kp_{\mathrm{F}}}-\frac{k}{2p_{\mathrm{F}}}\right]^2\right)\quad \omega_1\le\omega\le\omega_2$ $0\quad \omega_2\le\omega$	$\omega_1 = \frac{p_{\mathrm{F}}k}{m}-\frac{k^2}{2m}$ and $\omega_2 = \omega \le \frac{p_{\mathrm{F}}k}{m}+\frac{k^2}{2m}$

Bibliography

[1] S. Chu, *Nobel Lecture: The manipulation of neutral particles*, Rev. Mod. Phys. **70**, 685 (1998).

[2] C. N. Cohen-Tannoudji, *Nobel Lecture: Manipulating atoms with photons*, Rev. Mod. Phys. **70**, 707 (1998).

[3] W. D. Phillips, *Nobel Lecture: Laser cooling and trapping of neutral atoms*, Rev. Mod. Phys. **70**, 721 (1998).

[4] The Nobel Foundation, *The Nobel Prize in Physics 2001*, http://www.nobel.se/ physics/laureates/2001/

[5] C. J. Pethick and H. Smith, *Bose-Einstein Condensation in Dilute Gases*, (Cambridge University Press, 2001).

[6] L. Van Hove, *Correlations in Space and Time and Born Approximation Scattering in Systems of Interacting Particles*, Phys. Rev. **95**, 249 (1954).

[7] F. Dalfovo, S. Giorgini, L. P. Pitaevskii, and S. Stringari, *Theory of Bose-Einstein condensation in trapped gases*, Rev. Mod. Phys. **71**, 463 (1999).

[8] W. Ketterle, D. S. Durfee, and D.M. Stamper-Kurn, *Making, probing and understanding Bose-Einstein condensates*, The Proceedings of the 1998 Enrico Fermi summer school on Bose-Einstein condensation in Varenna (IOS Press, Amsterdam,1999), e-print arXiv:cond-mat/9904034 (1999).

[9] M. R. Andrews, *Bose gases and their Fermi cousins*, Nature **398**, 195 (1999).

[10] M.-O. Mewes, M. R. Andrews, D. M. Kurn, D. S. Durfee, C. G. Townsend, and W. Ketterle, *Output Coupler for Bose-Einstein Condensed Atoms*, Phys. Rev. Lett. **78**, 582 (1997).

[11] M.-O. Mewes, G. Ferrari, F. Schreck, A. Sinatra, and C. Salomon, *Simultaneous magneto-optical trapping of two lithium isotopes*, Phys. Rev. A **61**, 011403 (2000).

[12] A. W. Hagley, L. Deng, M. Kozuma, J. Wen, K. Helmerson, S. L. Rolston, and W. D. Phillips, *A Well-Collimated Quasi-Continuous Atom Laser*, Science **283**, 1706 (1999).

[13] A.-P. Jauho, *Coulomb drag between parallel two-dimensional electron systems*, Phys. Rev. B **47**, 4420 (1993).

[14] A. L. Fetter and J. D. Walecka, *Quantum Theory of Many-Particle Systems*, (McGraw-Hill, New York, 1971).

[15] C. R. Monroe, E. A. Cornell, C. A. Sackett, D. J. Myatt, and C. E. Wieman, *Measurement of Cs-Cs- Elastic Scattering at T=30 μK*, Phys. Rev. Lett. **70**, 414 (1993).

[16] J. L. Bohn, *Cooper pairing in ultracold ^{40}K using Feshbach resonances*, Phys. Rev. A **61**, 053409 (2000).

[17] K. B. Davis, M.-O. Mewes, M. R. Andrews, N. J. van Druten, D. S. Durfee, D. M. Kurn, and W. Ketterle, *Bose-Einstein condensation in a gas of sodium atoms*, Phys. Rev. Lett. **82**, 4208 (1999).

[18] C. N. Cohen-Tannoudji and W. D. Phillips, *New Mechanisms for Laser Cooling*, Physics Today **10**, 33 (1990).

[19] A. P. Chikkatur, A. Görlitz, D. M. Stamper-Kurn, S. Inouye, S. Gupta, and W. Ketterle, *Suppression and Enchancement of Impurity Scattering in a Bose-Einstein Condensate*, Phys. Rev. Lett. **85**, 483 (2000).

[20] R. Onofrio, C. Raman, J. M. Vogels, J. Abo-Shaeer,A. P. Chikkatur, and W. Ketterle, *Observation of Superfluid Flow in a Bose-Einstein Condensed Gas*, Phys. Rev. Lett. **85**, 2228 (2000).

[21] D. M. Stamper-Kurn, A. P. Chikkatur, A. Görlitz, S. Inouye, S. Gupta, D. E. Pritchard, and W. Ketterle, *Excitation of Phonons in a Bose-Einstein Condensate by Light Scattering*, Phys. Rev. Lett. **83**, 2876 (1999).

[22] W. Ketterle, and S. Inouye, *Collective enchancement and suppression in Bose-Einstein condensate, Notes from Summer School on Bose-Einstein condensates and atom lasers, Cargese, Corse, 2000*, Compte rendus de l'académie des sciences, Série IV, vol. 2.,339 (2001), e-print arXiv:cond-mat/0101424.

[23] B. DeMarco, J. L. Bohn, J. P. Burke, Jr., M. Holland, and D. S. Jin, *Measurement of p-Wave Threshold Law Using Evaporatively Cooled Fermionic Atoms*, Phys. Rev. Lett. **82**, 4208 (1999).

[24] H. F. Hess, *Evaporative cooling of magnetically trapped and compressed spin-polarized hydrogen*, Phys. Rev. B **34**, 3476 (1986).

[25] D. M. Giltner, R. W. McGowan, and S. A. Lee, *Atom Interferometer Based on Bragg Scattering from Standing Light Waves*, Phys. Rev. Lett. **75**, 2638 (1995).

[26] J. Y. Courtois, G. Grynberg, B. Lounis, and P. Verkerk, *Recoil-induced resonances in cesium: An atomic analog to the free-electron laser*, Phys. Rev. Lett. **72**, 3017 (1994).

[27] B. DeMarco and D. S. Jin, *Onset of Fermi Degeneracy in a Trapped Atomic Gas*, Science **285**, 1703 (1999).

[28] A. G. Truscott, K. E. Strecker, W. I. McAlexander, G. B. Partridge, R. G. Hulet, *Observation of Fermi Pressure in a Gas of Trapped Atoms*, Science **291**, 2570 (2001).

[29] Z. Hadzibabic, C. A. Stan, k. Dieckmann, S. Gupta, M. W. Zwierlein, A. Görlitz, and W. Ketterle, *Two-species mixture of quantum degenerate Bose and Fermi gases*, e-print arXiv:cond-mat/112425 (2001).

[30] K. M. O'Hara, M. E. Gehm, S. R. Granade, S. Bali, and J. E. Thomas, *Stable, Strongly Attractive, Two-State Mixture of Lithium Fermions in an Optical Trap*, Phys. Rev. Lett. **85**, 2092 (2000).

[31] B. DeMarco, S. B. Papp, and D. S. Jin, *Pauli Blocking of Collisions in a Quantum Degenerate Atomic Fermi Gas*, Phys. Rev. Lett. **86**, 5409 (2001).

[32] Idziaszek, L. Santos, and M. Lewenstein, *Laser cooling of trapped Fermi gases far below the Fermi temperature*, Phys. Rev. A **64**, 051402(R) (2001).

[33] J. Ruostekoski and J. Javanainen *Optical Linewidth of a Low Density Fermi-Dirac Gas*, Phys. Rev. A **82**, 4741 (1999).

[34] J. Javanainen, *Spectrum of Light Scattered from a Degenerate Bose Gas*, Phys. Rev. Lett. **75**, 1927 (1995).

[35] J. Javanainen, and J. Ruostekoski *Off-resonance light scattering from low-temperature Bose and Fermi gases*, Phys. Rev. A **52**, 3033 (1995).

[36] B. DeMarco and D. S. Jin, *Exploring a quantum degenerate gas of fermionic atoms*, Phys. Rev. A **58**, 4267 (1998).

[37] G. Ferrari, *Collisional relaxation in a fermionic gas*, Phys. Rev. A **59**, 4125 (1999).

[38] S.-K. Yip and Tin-Lun Ho, *Zero sound modes of dilute Fermi gases with arbitrary spin*, Phys. Rev. A **59**, 4653 (1999).

[39] M. J. Holland, B. DeMarco, and D. S. Jin, *Evaporative cooling of a two-component degenerate Fermi gas*, Phys. Rev. A **61**, 053610 (2000).

[40] M. Houbiers, R. Ferwerda, H. T. C. Stoof, W. I. McAlexander, C. A. Sackett, and R. G. Hulet *Superfluid state of atomic ^6Li in a magnetic trap*, Phys. Rev. A **56**, 4864 (1997).

[41] H. T. C. Stoof, M. Houbiers, C. A. Sackett, and R. G. Hulet *Superfluidity of Spin-Polarized ^6Li*, Phys. Rev. A **76**, 10 (1996).

[42] M. Mackie, J. Piilo, K.-A. Suominen, and J. Javanainen, *Coherent control of superfluidity in a Fermi gas of atoms*, e-print arXiv:physics/0104043 (2001).

[43] W. Ketterle and S. Inouye, *Does Matter Wave Amplification Work for Fermions?*, Phys. Rev. Lett. **86**, 4203 (2001).

[44] A. J. Leggett, *Scattering of light and atoms in a Fermi-Dirac gas with Bardeen-Cooper-Schrieffer pairing*, Phys. Rev. A **61**, 033605 (2000).

[45] W. Zhang, C. A. Sackett, and R. G. Hulet, *Optical detection of a Bardeen-Cooper-Schrieffer phase transition in a trapped gas of fermionic atoms*, Phys. Rev. A **60**, 10 (1999).

[46] J. Ruostekoski, *Scattering of light and atoms in a Fermi-Dirac gas with Bardeen-Cooper-Schrieffer pairing*, Phys. Rev. A **61**, 033605 (2000).

[47] J. Ruostekoski, *Optical response of a superfluid state in dilute atomic Fermi-Dirac gases*, Phys. Rev. A **60**, 1775 (1999).

[48] G. M. Bruun, P. Törmä, M. Rodriquez, and P. Zoller, *Laser probing of Cooper-paired trapped atoms*, Phys. Rev. A **64**, 033609 (2001).

[49] J. Stenger, S. Inouye, A. P. Chikkatur, D. M. Stamper-Kurn, D. E. Pritchard, and W. Ketterle, *Bragg Spectroscopy of a Bose-Einstein Condensate*, Phys. Rev. Lett. **82**, 4569 (1999).

[50] P. J. Martin, B. G. Oldaker, A. H. Miklich, and D. E. Pritchard, *Bragg scattering of atoms from a standing light wave*, Phys. Rev. Lett. **60**, 515 (1988).

[51] M. Kozuma, L. Deng, E. W. Hagley, J. Wen, R. Lutwak, K. Helmerson, S. L. Rolston, and W. D. Phillips, *Coherent Splitting of Bose-Einstein Condensed Atoms with Optically Induced Bragg Diffraction*, Phys. Rev. Lett. **82**, 871 (1999).

[52] H. A. Gersch, L. J. Rodriquez, and P. N. Smith, *Corrections to the Impulse Approximation for High-Energy Neutron Scattering from Liquid Helium*, Phys. Rev. A **5**, 1547 (1972).

[53] B. P. Blakie and R. J. Ballagh, *Theory of coherent Bragg spectroscopy of a trapped Bose-Einstein condensate*, e-print arXiv:cond-mat/0108480 (2001).

[54] A. Brunello, *Momentum transferred to a trapped Bose-Einstein condensate by stimulated light scattering*, e-print arXiv:cond-mat/0104051 (2001).

[55] R. K. Pathria, *Statistical Mechanics*, (Butterworth, Heinemann, Oxford, 1996).

[56] D. Pines and P. Nozières, *The Theory of Quantum Liquids, Vol I*, (W. A. Benjamin, New York, 1966).

[57] D. Pines and P. Nozières, *The Theory of Quantum Liquids, Vol II*, (Addison-Wesley Publishing Co., New York, 1990).

[58] B. Vacchini, *Test particle in a quantum gas*, Phys. Rev. B **63**, 066115 (2001).

[59] F. Zambelli, L. Pitaevskii, D. M. Stamper-Kurn, and S. Stringari, *Dynamic structure factor and momentum distribution of a trapped Bose gas*, Phys. Rev. A **61**, 063608 (2000).

[60] F. Mazzanti, A. Polls, *Finite temperature dynamic structure function of the free Bose gas*, Phys. Lett. A **257**, 1 (1999).

[61] F. Mazzanti, A. Polls, *Finite temperature dynamic structure function of the free Fermi gas*, Phys. Lett. A **263**, 416 (1999).

[62] G. Baym, C. J. Pethick, M. Salomaa, *Mobility of Negative Ions in Superfluid ^{3}He-B*, J. Low Temp. Phys. **36**, 431 (1979).

[63] A. B. Kuklov and B. V. Svistunov, *Testing quantum correlations in a confined atomic cloud by the scattering of fast atoms*, Phys. Rev. A **60**, R769 (1999).

[64] M. D. Girardeau and E. M. Wright, *Measurement of One-Particle Correlations and Momentum Distributions for Trapped 1D Gases*, Phys. Rev. Lett. **87**, 050403 (2001).

[65] F. Schreck, L. Khaykovich, K.L. Corwin, G. Ferrari, T. Bourdel, J. Cubizolles, and C. Solomon, *Quasipure Bose-Einstein Condensate Immersed in a Fermi Sea*, Phys. Rev. Lett. **87**, 080403 (2001).

[66] L. Pitaevskii and S. Stringari, *Interference of Bose-Einstein Condensates in Momentum Space*, Phys. Rev. Lett. **83**, 4237 (1999).

Sources of the quoted images

[67] *http://www.aip.org/physnews/graphics/images/fermisur.gif*

[68] *http://spot.colorado.edu/~cwieman/images/cond.gif*

[69] *http://physics.nist.gov/MajResProj/QuantumInfo/Images/JILA3peak.jpg*

[70] *http://www.nist.gov/public_affairs/taglance/bose.jpg.*